HHS Public Access

Author manuscript

Cell Stem Cell. Author manuscript; available in PMC 2024 August 03.

Published in final edited form as:

Cell Stem Cell. 2023 August 03; 30(8): 1091–1109.e7. doi:10.1016/j.stem.2023.07.002.

Tff2 defines transit-amplifying pancreatic acinar progenitors that lack regenerative potential and are protective against Kras-driven carcinogenesis

Zhengyu Jiang[1,5,14], **Feijing Wu**[1,6,14], **Pasquale Laise**[2,7], **Tanaka Takayuki**[1], **Fu Na**[1,8], **Woosook Kim**[1], **Hiroki Kobayashi**[1], **Wenju Chang**[1], **Ryota Takahashi**[1], **Giovanni Valenti**[1], **Masaki Sunagawa**[1], **Ruth A. White**[4], **Marina Macchini**[1], **Bernhard W. Renz**[1,9], **Moritz Middelhoff**[1,10], **Yoku Hayakawa**[11], **Zinaida Dubeykovskaya**[1], **Xiangtian Tan**[2], **Timothy Chu**[1], **Karan Nagar**[1], **Yagnesh Tailor**[1], **Bryana R Belin**[1], **Akanksha Anand**[12], **Samuel Asfaha**[13], **Michael O Finlayson**[2], **Alina C Iuga**[3], **Andrea Califano**[2,7], **Timothy C Wang, M.D.**[1,*]

[1]Division of Digestive and Liver Diseases, Department of Medicine, College of Physicians and Surgeons, New York, USA;

[2]Department of Systems Biology, College of Physicians and Surgeons, New York, USA;

[3]Department of Pathology and Cell Biology, College of Physicians and Surgeons, New York, USA;

[4]Division of Hematology and Oncology, College of Physicians and Surgeons, New York, USA;

[5]Currennt address: Janssen Research and Development, Johnson & Johnson, PA, USA;

[6]The Second Affiliated Hospital of Fujian Medical University, Quanzhou, Fujian, China;

[7]DarwinHealth Inc, New York, NY, USA;

[8]Department of Traditional and Western Medical Hepatology, Third Hospital of Hebei Medical University, Shijiazhuang, China;

[9]Department of General, Visceral, and Transplantation Surgery, LMU University Hospital, LMU Munich, Germany;

[10]Division of Digestive and Liver Diseases, CU and Klinikum rechts der Isar, Technical University, Munich, Germany;

[*]**Corresponding author and Lead contact:** Timothy C. Wang, M.D., Division of Digestive and Liver Diseases, Columbia University Medical Center, 1130 St. Nicholas Avenue, New York, NY 10032 USA, Phone: (212) 851 4581, Fax: (212) 851 4590, tcw21@columbia.edu.

AUTHOR CONTRIBUTIONS

Conceptualization, Z.J. and T.C.W.; Methodology, Z.J. and T.C.W.; Software: P.L.; Formal Analysis, Z.J., F.W., P.L. and M.O.F.; Investigation, Z.J., F.W., P.L., T.T., F.N., W.K., H.K., W.C., R.T., G.V., M.S., R.A.W., X.T., M.M., B.W.R., M.M., Y.H., Z.D., T.C., K.N., Y.T., B.R.B., A.A., A.C.I.; Resources, S.A.; Writing – Original Draft, Z.J.; Writing – Review & Editing, Z.J., F.W., P.L., A.C. and T.C.W.; Supervision, T.C.W.; Funding Acquisition, T.C.W.

DECLARATION OF INTERESTS

P.L. is Sr. Director of Single-Cell Systems Pharmacology at DarwinHealth, Inc., a company that has licensed some of the algorithms used in this manuscript from Columbia University. A.C. is founder, equity holder, and consultant of DarwinHealth Inc. Columbia University is also an equity holder in DarwinHealth Inc.

[11]Graduate School of Medicine, Department of Gastroenterology, The University of Tokyo, Tokyo, Japan;

[12]Division of Digestive and Liver Diseases, Department of Medicine and Department of Gastroenterology II, Klinikum rechts der Isar, Technical University, Munich, Germany;

[13]Department of Medicine, Schulich School of Medicine and Dentistry, Western University, London, Ontario, Canada;

[14]These authors contributed equally

Summary

While adult pancreatic stem cells are thought not to exist, it is now appreciated that the acinar compartment harbors progenitors, including tissue-repairing facultative progenitors (**FP**s). Here, we study a pancreatic acinar population marked by trefoil factor 2 (**Tff2**) expression. Long-term lineage tracing and single-cell RNA-seq analysis of *Tff2-DTR-CreER*^{T2}-targeted cells defines a transit-amplifying progenitor (**TAP**) population that contributes to normal homeostasis. Following acute and chronic injury, Tff2^{+} cells, distinct from FPs, undergo depopulation but are eventually replenished. At baseline, oncogenic Kras^{G12D} targeted Tff2^{+} cells are resistant to PDAC initiation. However, Kras^{G12D} activation in Tff2^{+} cells leads to survival and clonal expansion following pancreatitis and a cancer stem/progenitor cell-like state. Selective ablation of Tff2^{+} cells prior to Kras^{G12D} activation in Mist1^{+} acinar or Dclk1^{+} FP cells results in enhanced tumorigenesis, which can be partially rescued by adenoviral Tff2 treatment. Together, Tff2 defines a pancreatic TAP population that protects against Kras-driven carcinogenesis.

Graphical Abstract

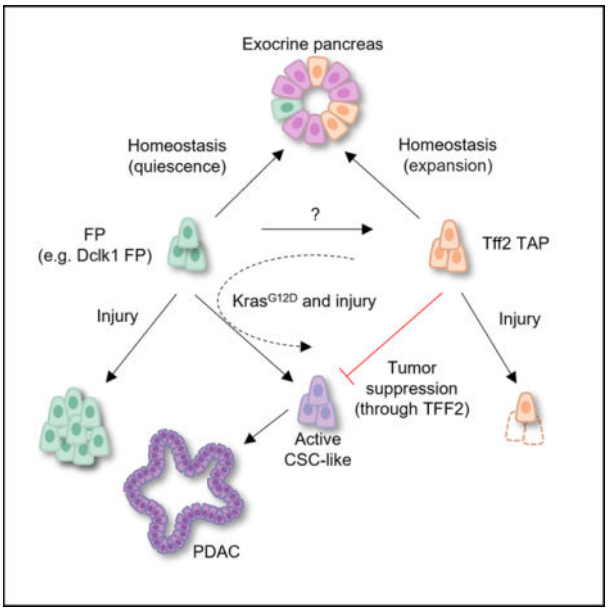

In brief

Jiang and Wu et al. discover Tff2$^+$ pancreatic acinar TAPs. They investigate Tff2$^+$ TAP behavior in homeostasis, injury and cancer, revealing their lack of regenerative capacity, resistance to oncogene activation, and their protective role against tumorigenesis.

Keywords

Trefoil factor 2; transit-amplifying cells; progenitor cells; pancreas; regeneration; pancreatic ductal carcinoma; lineage tracing; cell ablation

INTRODUCTION

While the adult pancreas is believed not to harbor multipotent stem cells, pancreatic progenitors are well established. In embryonic development, a cell lineage hierarchical relationship has been delineated, with multipotent embryonic progenitors serving as precursors for acinar, duct and endocrine cell lineages.[1,2] Nevertheless, such multipotent progenitors are largely absent or restricted after birth.[3,4] Mathematical modeling proposed an acinar self-replication model, suggesting a uniform progenitor potential[5] and self-replication of pre-existing terminally differentiated acinar cells believed to drive homestasis and regeneration.[6] However, most experimental model systems have been unable to adequately test or confirm this self-replication model, and recent lineage-tracing studies have identified in the adult pancreas distinct acinar-derived regenerative progenitor cells marked by Bmi1, Stmn, Tert or Dclk1.[7–10] Interestingly, these facultative progenitors (**FP**s) demonstrate discrete molecular identity and a variable capacity to expand in response to injury.[11,12] Dclk1$^+$ FPs, in particular, lineage trace much of the acinar compartment following injury, and their absence impairs pancreatic regeneration.[9] However, FP populations are largely quiescent and contribute little to normal tissue homeostasis. Thus, homeostasis of the normal pancreas may be maintained, in contrast to the self-replication model, by more active (*e.g.*, "transit-amplifying" or **TA**) progenitors, which are a proliferative but lineage restricted population; in the skin, they are described as an undifferentiated population in transition between stem cells and differentiated cells.[13] Single-cell RNA sequencing efforts have confirmed extensive molecular heterogeneity in pancreatic acinar cells[8,14], suggesting complexity to the progenitor pool and the possible existence of additional cellular sources for pancreatic homeostasis (also see review[15]).

The vast majority of cancers arise due to accumulated genetic mutations acquired during cell division.[16] In numerous organs, the susceptibility of a diverse progenitor cell compartment to oncogenic alternations has demonstrated non-equipotency. Recent studies of skin epidermis showed that oncogenic hedgehog (HH)-targeted stem cells readily progress to basal cell carcinoma, while committed progenitors are restricted to dysplasia.[17] In the pancreas, oncogenic Kras activation plays a key role in potentiating the development of pancreatic ductal adenocarcinoma (**PDAC**).[18] However, it remains unresolved whether Kras-driven PDAC arises more from unidentified stem cells, active or facultative progenitors, or terminally differentiated cells that might undergo dedifferentiation. Lineage tracing studies have shown that the acinar compartment harbors a diverse pool of progenitors that serve as a cellular source for PDAC, with greater susceptibility to Kras transformation compared

to ductal cells.[19,20] In the context of liver, periportal hepatocytes are highly efficient in regenerating injured livers but are not capable of giving rise to hepatocellular carcinoma.[21] Thus, despite a strong link between tissue injury and cancer[22], the cellular sources for tissue regeneration and cancer initiation may not be identical. Questions of whether and how diverse progenitor cell populations in the pancreas respond to injury or oncogenic activation remain elusive.

The link between trefoil factor 2 (**Tff2**, originally termed "pancreatic spasmolytic polypeptide") to a gastric multipotent progenitor cell population[23] led us to investigate Tff2-expressing cells in the pancreas. TFF2 shows detectable expression in both embryonic and adult pancreas, with altered expression in diseased states.[24,25] Knockout of Tff2 in mice promotes colonic, gastric, and pancreatic tumorigenesis, demonstrating a suppressive role of TFF2 in mouse models of cancer.[26–28] While TFF2 is most abundantly expressed in the gastric mucosa, TFF2 was actually first discovered in the pig pancreas[29], and was subsequently confirmed to be strongly expressed in porcine acinar cells[30] and in mucin-producing pancreatic tumors in human.[31,32] To date, the exact cellular and lineage identity of Tff2-expressing cells in the pancreas has remained unsettled. We show here that high levels of Tff2 transcripts are expressed in scattered murine pancreatic acinar cells that are active progenitors contributing to tissue homeostasis. Furthermore, we demonstrate that, in contrast to FPs, the $Tff2^{+}$ progenitor population is highly susceptible to tissue injury, does not drive regeneration, is resistant to oncogene-activation, but plays essential roles in protecting the pancreas from tumorigenesis.

RESULTS

Tff2 labels a subset of pancreatic acinar population that is distinct from Dclk1 FPs

To investigate pancreatic Tff2-expressing cells, we generated an inducible *Tff2-DTR-CreER^{T2}* mouse through modification of a *BAC* allele. We crossed the *Tff2-DTR-CreER^{T2}* line with reporter mice (*R26-mTmG* or *R26-tdTomato/RFP* strains). Following tamoxifen (**TM**) induction, we evaluated Tff2 tracing in the adult pancreas (Figure 1A–1B). To validate *Tff2-DTR-CreER^{T2}* tracing, we analyzed endogenous Tff2/TFF2 expression of fluorescence-activated cell sorting (**FACS**)-sorted recombined cells by RT-qPCR and ELISA, and confirmed expression enrichment (Figure S1A–S1C). To exclude potential Cre leakage, we assessed the *Tff2-DTR-CreER^{T2}; R26-mTmG* mice without TM induction at 12 months, and confirmed the absence of random reporter recombination (Figure S1D and S1E). One week after TM induction, recombination was mostly confined to the acinar compartment (mostly co-localization with amylase, Figure 1C and 1D-i), with only rare reporter tracing in centroacinar cells (**CAC**, Figure S1F and S1G); reporter tracing was entirely absent in pancreatic islets and rarely expressed or absent in ducts (>100 islets showed absent tracing for up to 1.5 years, Figure 1C, 1D-iii, 1H, and S1H–J). While the vast majority (>90%) of Tff2 labeled cells co-stained with Mist1 (Figure 1C, 1D-ii, and 1H), known to mark pancreatic acinar cells[33], around 5% of the Tff2 labeled cells expressed low levels of Sox9, an established progenitor marker[34] (Figure 1C, 1D-iv, and 1H). In addition, fluorescent RNAScope® ISH analysis of Tff2 mRNA in the mouse pancreas deomonstrated

that the majority of acinar cells were Tff2^{-}, while up to 8% of acinar subpopulation was Tff2^{+} (Figure 1I–1L).

To address whether *Tff2-DTR-CreER^{T2}*-targeted cells are distinct from quiescent FPs marked by Dclk1[9], we crossed the *Tff2-DTR-CreER^{T2}* line with a recently generated *Dclk1-ZsGreen-DTR BAC* reporter mouse (**see** Methods). Interestingly, none of the recombined Tff2^{+} cells overlapped with Dclk1^{+} cells, as revealed by immunofluorescence (**IF**) and FACS analysis of whole pancreas (Figure 1E–1G), suggesting that *Tff2-DTR-CreER^{T2}* indeed marks a lineage distinct from Dclk1-expressing cells.

To determine whether progenitor and CAC markers are enriched in RFP^{+} (Tff2^{+}) cells, FACS-sorted RFP^{+}, RFP^{-} acinar cells and ductal cells were analyzed for mRNA expression of c-Met, Aldh1a1 and Aldh1a7 by RT-qPCR. Compared to RFP^{-} acinar cells, expression of c-Met was elevated in RFP^{+} cells (Figure S1K–S1M). However, Aldh1a7 but not Aldh1a1 was elevated in the RFP^{+} population, suggesting that Tff2^{+} cells likely overlap a CAC subset.

Tff2-DTR-CreER^{T2} targets transit-amplifying progenitors (TAP)

Cellular turnover in adult pancreas proceeds at a very slow pace, with replacement averaging approximately 4 months.[35] To evaluate the cellular dynamics of Tff2^{+} cells quantitatively, we analyzed lineage tracing at ten separate time points, ranging from 2 days to 18 months post-induction, a period of time spanning three-quarters of the murine lifetime (Figure 2A). We utilized *Tff2-DTR-CreER^{T2}; R26R-mTmG* transgenic mice and identified Tff2-expressing cells through green fluorescence. Two days post-induction, recombined cells were distributed throughout the pancreas, comprising about 2% of the overall pancreas (Figure 2B–2C and S2A–S2F). Under these conditions of homeostasis, Tff2-expressing cells showed moderate levels of proliferation, resulting in a slow but statistically significant expansion, peaking at 6 months. At this maximum point of expansion, *Tff2-DTR-CreER^{T2}* traced descendants comprised nearly 10% of pancreatic epithelium (Figure 2B and 2C). In contrast to Dclk1^{+} FPs, which persist as single cells and only rarely produce cell clusters[9], an increasing number of Tff2 progeny over time were found within expanded clones (Figure 2D and 2E), with a gradual loss of recombined single clones. At 6 months post-induction, up to 40% of clones completed one round of cell division. After 6 months, there was a decrease in the rate in new cluster formation, along with a progressive loss of Tff2^{+} cells, with the majority of surviving clones persisting as single-cell clones. Taken together, these observations indicate that *Tff2-DTR-CreER^{T2}* targeted cells follow an expansion pattern expected of TAP cells that contribute to epithelial maintenance.

To further confirm the proliferative activity of Tff2 labeled cells, we subjected *Tff2-DTR-CreER^{T2}*; *R26-tdTomato* mice to continuous 5-Bromo-2'-deoxyuridine (*BrdU*) treatment for one month (Figure 2F and S2G). Although there was a greater total number of *BrdU*$^{+}$ RFP^{-} cells, the percentage of *BrdU* positivity was much greater in RFP^{+} cells vs. RFP^{-} cells (>100 fold, Figure 2G and 2H), indicating that Tff2^{+} cells were much more proliferative. In addition, analysis of the constitutive *Tff2-Cre* line (activated in the late embryonic development, Figure S2I–S2K) crossed with *R26-Rainbow2.1* mice revealed significant clonal expansion of Tff2^{+} cells, which over an 18-month period repopulated over 40%

of pancreatic epithelium, with a progressive decrease in single-cell clones (Figure 2I–K and S2H). These expanded clones appear to be confined to the acinar compartment, as demonstrated by immunostaining for CK19 (duct) and Chromogranin A (islet), which showed no overlapping signals but *Tff2-Cre* tracing instead co-localized with amylase (Figure S2L and S2M). Although $Tff2^+$ embryonic progenitors may not be identical to adult $Tff2^+$ progenitors, the 4-fold increase in labeled cells between 6 weeks and 18 months strongly supported the presence of an active progenitor, with long-term replenishment of pancreatic acini.

Molecular characterization of the $Tff2^+$ cellular population by scRNAseq analysis

To characterize at a molecular level the *Tff2-DTR-CreERT2* targeted cells, we profiled by single-cell RNA sequencing (**scRNA-seq**) the FACS-purified $TER119^-CD45^-EpCAM^+RFP^+$ cells at 96 hours after TM administration (Figure 3A). After filtering sequenced cells with low-quality reads, the scRNA-seq profile of 922 high-quality cells were used to generate a context-specific regulatory network using the ARACNe algorithm, an experimentally validated algorithm for inferring transcriptional interaction from gene expression data (**see** Methods)[36–38]. ARACNe identified transcriptional targets of large set (n=2774) of regulatory proteins (**RP**s) including transcription factors (**TF**s), co-transcription factors (**coTF**s) and signaling molecules (**SigMol**) (Supplementary Excel Table 3). Gene expression levels of the ARACNe-inferred transcriptional targets of a given RP can be used as multiplexed gene reporter assay to assess its transcriptional activity using the VIPER algorithm, which, for simplicity, is termed as protein activity. Therefore, VIPER-based scRNAseq analysis quantitates single-cell protein activity from gene expression data.[39] Furthermore, VIPER-implemented protein activity-based clustering overcomes the limitation of expression-based clustering and increases the robustness and resolution.[40]

Unsupervised clustering based on VIPER-inferred protein activity (using Louvain algorithm with resolution parameter optimized based on silhouette analysis) identified four clusters (0, 1, 2, 3) with distinct protein activity that correlate with Tff2 transcriptional levels (Figure S3A and S3B). However, we excluded clusters 2 and 3 from further analysis due to biomarker enrichment of immune (cluster 2) and endothelial cell identity (cluster 3) and fairly low Tff2 gene expression (Figure S3C–S3I). To predict cellular differentiation, single-cell entropy analysis was performed, demonstrating that cells in cluster 0 are less differentiated compared to the cells in cluster 1 (Figure 3B and S3C). Cluster 1 showed higher activity levels of Bhlha15 (Mist1) and Cckar, while cluster 0 showed higher levels of Runx2, Mapk1 and Top2A, regulators involved in cell differentiation (Figure 3D–3H). In addtion, gene set enrichment analysis by EnrichR[41] of the most differentially activated regulators revealed significant enrichment for TGF-β, Wnt and Notch signaling pathways in cluster 0 but not in cluster 1 (Figure 3I), suggesting the presence of a potential cellular differentiation trajectory.[42–44] Furthermore, pseudotrajectory analysis predicted a path from least differentiated cells in cluster 0 to the most differentiated cells in cluster 1, matching the pattern of sc-entropy analysis (Figure 3J and 3K). Finally, we interrogated the cellular differentiation trajectory with Tff2 mRNA levels. Strikingly, this analysis identified the subset of cells predicted to be the least differentiated (highlighted by the density analysis in the pseudotrajectory space) as the cells expressing the lowest levels of Tff2 (Figure

3L). Together, these analyses suggested that Tff2 mRNA levels correlated with the cellular differentiation states of RPF^+ acinar population and that $Tff2^{moderate}$ acinar cells associated with a low differentiated progenitor-like state.

To demonstrate the differentiation capacity of Tff2 progenitor cells, we enumerated the binuclear $mGFP^+$ (Tff2) cells in the abovementioned time-course lineage-tracing experiment. Binuclear acinar cells, resistant to cell cycle entry, are defined as terminally-differentiated acinar cells.[8] Our results showed a significant increase in both the total number and percentage of binuclear $mGFP^+$ cells at days 90, 180 and 365 compared to day 2 (Figure S3J–S3L). In addition, FACS-sorted Tff2-traced RFP^+ cells at 60 days post TM exhibited increased gene expression of amylase and cckar, markers mostly expressed by differentiated acinar cells, compared to day 2 (Figure 3M–3P). Lack of detectable expression of the differentiated ductal gene marker CFTR was observed in both days 60 and 2, indicating the absence of ductal differentitation (Figure S3M). Immunostaining of amylase also confirmed an increase in percentage of $amylase^+RFP^+$ cells on day 60 (Figure S3N–S3O). These data provided evidence that Tff2 progenitor cells undergo acinar differentiation over time.

Distinct from FPs, Tff2 TAPs are susceptible to injury

Previous studies indicated that several acinar cell subpopulations can expand and regenerate the exocrine pancreas after injury.[7–9] To test the regenerative capacity of $Tff2^+$ cells, we analyzed lineage tracing events from *Tff2-DTR-CreER^{T2}* targeted cells in injury models. Tamoxifen was administered 48 hours prior to caerulein treatment or pancreatic duct ligation (**PDL**). Surprisingly, caerulein-induced pancreatitis resulted in a marked reduction in traced $Tff2^+$ cells, with a >80% decrease in total recombined cells compared with PBS-treated control mice (Figure 4A–4C). PDL led to an even more substantial loss of recombined $Tff2^+$ cells, with a >90% decrease in traced cells compared to sham-ligated controls (Figure S4A–S4C). However, in the partial pancreatectomy (**Ppx**) model, we did not observe any significant reduction in $Tff2^+$ cells, although there was also no significant expansion of tracing (Figure S4D–S4F), which contrasts with $Dclk1^+$ cells that undergo extensive expansion after Ppx[9]. In addition, there was a substantial depopulation of the $Tff2^+$ cells in chronic injury induced by daily caerulein injections (Figure 4D–4F). Thus, in response to acute or chronic pancreatic injury, $Tff2^+$ TAPs do not contribute to regeneration but instead are mostly lost.

Active stem or progenitor cells are often vulnerable to injury but later replenishable from quiescent stem cells or reserve progenitors through interconversion.[45] To test if $Tff2^+$ TAPs are similarly replenished during tissue repair, we re-administered TM at 2, 4, 7, or 12 days during the regenerating phase of caerulein injury.[12] Interestingly, TM doses given at the later time points of 7 or 12 days post-injury yielded 2–4 fold increases in total cellular recombination (Figure 4G–4I). This result was not due to the multiple TM treatments since giving one or three earlier pulses of TM administration resulted in the same level of total recombination (Figure S4G and S4H). Together, these data suggest that, distinct from previously reported acinar progenitors, pre-existing $Tff2^+$ TAPs do not serve as a driver

for pancreatic regeneration but are nevertheless replenishable during regeneratoin following injury.

Oncogene-targeted Tff2$^+$ TAPs do not progress to PDAC but are converted to more active or long-lived progenitors

In some organs, stem cells but not committed progenitors efficiently initiate cancers, while in others progenitors are conditionally transformable during carcinogenesis.[17,46] To determine whether the Tff2$^+$ TAPs are capable of efficiently giving rise to PDAC, a cohort of *Tff2-DTR-CreER^{T2}* mice were crossed with mice bearing the conditional oncogenic *LSL-Kras$^{G12D/+}$* allele. Animals were given three pulses of TM at 6 weeks postnatal in order to efficiently activate mutant Kras, and then followed for 3, 6, 12, and 18 months (Figure 5A). Targeted expression of the Kras^{G12D} allele in Tff2$^+$ cells led to the gradual formation of low-grade pancreatic intraepithelial neoplasia (**PanIN**s, 1 and 2) and papillary lesions (Figure 5A–5C and S5A–S5B). Although the proportion of animals with PanINs continued to increase slowly with aging, at 18 months post-induction, in contrast to other model systems, no PDAC was initiated and Kras^{G12D} targeted Tff2$^+$ cells were limited to producing early PanIN lesions. The addition of a mutant *LSL-Trp53$^{+/R172H}$* allele[47], which has been reported to enhance PDAC initiation where the *Kras^{G12D}* allele is insufficient, did not lead PDAC within one year (Figure 5D and 5E). Overall, these data suggest that Tff2$^+$ TAPs are more resistant to PDAC formation than other acinar populations (**see** Supplementary Table 1 **for comparisons**), irrespective of oncogene or tumor suppressor gene.

Since Tff2 TAPs show gradual reductions with aging, we asked if activation of Kras^{G12D} influences the lineage behavior. Intriguingly, when we examined lineage tracing in *Tff2-DTR-CreER^{T2}*; *LSL-Kras$^{G12D/+}$*; *R26-mTmG* mice at 21–22 months after TM induction, we observed an over 3-fold increase in Tff2 traced cells compared with *Tff2-DTR-CreER^{T2}*; *R26-mTmG* mice (Figure S5C–S5E). These data suggest that oncogene activation may convert Tff2$^+$ TAPs into more active and/or longer-lived progenitors.

Oncogene-targeted Tff2$^+$ TAPs progress to PDAC after pancreatitis

We also followed a cohort of *Dclk1-CreER^{T2}; LSL-Kras$^{G12D/+}$* mice[9] for 3–4 months and found that 77% (10/13) developed low grade PanINs (Supplementary Table 1). Since pancreatitis promotes tumorigenesis from FP cells, we investigated whether Tff2$^+$ TAPs, refractory to *Kras^{G12D}*-transformation, are able to progress to PDAC after pancreatitis. Indeed, upon caerulein treatment, the formation and progression of advanced PanIN lesions were dramatically accelerated (Figure 5F–5H and S5H). PanIN formation was observed in all animals as early as 3 months post induction (data not shown), while progression to PDAC was seen by 6 months. Overall, 36% of the animals developed aggressive PDAC (Figure 5H). A mortality rate of 14% was observed in the caerulein-treated mice (Figure 5H). The PDACs were primarily p53-inactivated (Figure S5F and S5G). Furthermore, to compare our Tff2 line with another acinar CreER line, we generated a cohort of *Elastase-CreER^{T2}*;*LSL-Kras^{G12D}* mice that were subjected to TM and caerulein. Histopathological analysis of the whole pancreas at 6 and 12 months post TM showed that up to 95% of the pancreas area was occupied by PanINs in Ela-Kras mice (n = 9–10), compared to a PanIN area of up to 61%

for Tff2-Kras mice (Figure SH). Lineage tracing of *Elastase-CreER^{T2}*; *R26-mTmG* mice showed that 48–60% of the pancreatic epithelium was recombined at one week or one month after TM induction (data not shown), compared to 2–8% for Tff2 mice. After calculating PanIN formation ability by PanIN area/labeling percentage[9], we found that the PanIN formation capacity of Tff2 line is approximately 3–5 fold higher than the Elastase line (Figure 5I), suggesting that Tff2 cells are more potent in tumorigenesis than the *Elastase-CreER^{T2}* cells after injury. Furthermore, when adjusted for labeling efficacy, the PDAC formation capacity of Tff2 mice is approximately 13 times higher than the Elastase mice (Figure 5K; Supplementary Table 1). Overall, while resistant to PanIN formation at baseline, Tff2^{+} TAPs became more susceptible in initiating pancreatitis-associated PDAC compared to acinar populations labeled by *Elastase-CreER^{T2}* and many other broadly expressed CreER lines (Supplementary Table 1). In addition, given the potential for inflammation-induced epigenetic reprograming of certain acinar progenitors such as Dclk1^{+} FP cells[48], we examined PanIN progression with or without caerulein treatment given 3 weeks prior to TM induction of Kras in the Tff2^{+} lineage. We found no PanIN formation after 3 months, similar to the non-treated group, suggesting that any pancreatitis-induced memory is not persistent in the Tff2 TAPs (Figure S5I and S5J).

Given the substantial effect of pancreatitis on potentiating Kras-driven tumorigenesis from Tff2^{+} cells, we next asked if pancreatitis promotes the transition of Tff2^{+} TAP cells into a more cancer-like stem cell (**CSC**) fate. FACS analysis of caerulein-treated pancreas after Kras^{G12D} activation in Tff2^{+} cells showed a significant increase in the CD44^{+}CD133^{+}CD24^{+} CSC population in the epithelial population (Figure 5L–5N). Immunostaining for CD44 confirmed the increase following caerulein treatment (Figure 5P). Gene expression analysis of caerulein-treated *Tff2-DTR-CreER^{T2}*; *LSL-Kras$^{G12D/+}$* pancreas demonstrated an increase in proliferation (Ki67) and stem cell markers including Aldh1b1, CD24, CD44, c-Myc, and CXCR4 (Figure 5O). Orthotopic transplantation of FACS-purified RFP^{+} epithelial cells from caerulein-treated *Tff2-DTR-CreER^{T2}*; *LSL-Kras$^{G12D/+}$*; *R26-tdtomoato* mice into NOD/SCID mice resulted in PanIN lesion formation, which was not seen in mice transplanted with RFP^{+} pancreatic epithelial cells from untreated animals (Figure 5Q and 5R). In addition, FACS-sorted epithelial cells demonstrated enhanced *in vitro* organoid forming ability in pancreatic cells from caerulein-treated animals compared to untreated controls (Figure 5S–5U). Furthermore, to address whether caerulein-induced CSC fate is a more general mechanism, we treated *Pdx1-Cre*; *LSL-Kras$^{G12D/+}$* (**KC**) mice with caerulein and found a similar expansion of the CSC cell population and increased CD44 expression compared to untreated KC mice (Figure S6A–S6E). To test whether the acquisition of a CSC-like state also relates to metaplastic changes associated with the acinar-to-ductal (**ADM**) transition, we evaluated the expression of ductal epithelial makers in RFP^{+} cells expressing mutant-KRAS from control or caerulean-treated mice. RT-qPCR data suggested that CFTR expression was elevated while amylase expression was decreased in caerulein-treated Tff2^{+} cells vs non-treated cells, suggesting that caerulein treatment overcomes resistance to mutant Kras-induced ADM in Tff2+ cells (Figure S6F and S6G).

Taken together, these observations suggest that pancreatitis converts Kras mutant Tff2^{+} progenitors into a state enriched for progenitor-like and/or CSC-like properties, facilitating progression toward tumorigenesis.

Oncogenic Kras prevents Tff2^{+} TAPs from caerulein-induced depopulation

Given that caerulein treatment led to reduced lineage tracing from normal Tff2^{+} progenitor cells, but strongly promoted PDAC from Kras mutant Tff2^{+} cells, we asked whether the expression of mutant Kras altered the response of Tff2^{+} cells to caerulein injury. Transgenic mice (*Tff2-DTR-CreER^{T2}*; *LSL-Kras$^{G12D/+}$*; *R26-mTmG*) were subjected to TM and caerulein treatment protocols and tracing events were analyzed at 0, 5, and 18 days after the last caerulein treatment (Figure 6A). As expected, oncogenic *Kras^{G12D}* activation significantly increased the survival of Tff2^{+} TAPs during the caerulein-induced injury phase and promoted greater clonal expansion during the recovery phase (Figure 6B–6D).

To further test whether Kras signaling plays an essential role in the survival and expansion of Tff2^{+} TAPs following injury, we treated the *Tff2-DTR-CreER^{T2}*; *LSL-Kras$^{G12D/+}$*; *R26-mTmG* mice with a MEK inhibitor, Trametinib, following the same TM and caerulein protocol (Figure 6E). Immunoblotting for pERK in the pancreas confirmed the inhibition of Kras signaling by Trametinib (Figure 6F). Further, the MEK inhibitor largely abolished the increased survival and expansion of Tff2 labeled cells by oncogenic Kras during both the injury and recovery phases (Figure 6G–6I). Since Trametinib has been reported not to interfere with caerulein-induced tissue damage[49], a possible compounding effect due to compromised tissue injury can be excluded. Altogether, these data suggest that oncogenic Kras signaling is sufficient to desensitize Tff2^{+} TAPs to caerulein-induced injury, such that the combination yields an enhanced potential of PDAC formation.

Tff2^{+} TAP are protective against Kras-driven tumorigenesis

While TFF2 has been shown to play a suppressor role in PDAC development[28], we investigated the role of Tff2-expressing cells in tumorigenesis through genetic cell ablation studies. We utilized the *Tff2-DTR-CreER^{T2}* transgenic allele, which was expressed almost exclusively in the pancreas and showed only minimal recombination in the stomach (Figure S7A and S7B). This allowed us to administer diphtheria toxin (**DT**) and to ablate pancreatic Tff2 cells without significantly affecting gastric homeostasis. We titrated the DT regimen to determine the minimum dose of DT that ablated >70% of Tff2^{+} cells (Figure S7C–S7E). The low dose of DT (10 ng) chosen for the expereiments had minimal histologic impact, with no evidence of inflammation (Figure S7F).

We generated double Cre transgenic mice, *Mist1-CreER^{T2};Tff2-DTR-CreER^{T2}*; *LSL-Kras$^{G12D/+}$* (***MTK***) and administered 10 ng of DT (x2) to these animals at three weeks prior to TM induction (Figure 7A). Subsequently, animals were treated with caerulein to initiate a uniform and robust PanIN formation. As controls for this experiment, we generated *Mist1-CreER^{T2}; Tff2-DTR-CreER^{T2}* mice with WT Kras (Figure 7B). In the setting of mutant Kras in the *MTK* mice, ablation of Tff2 cells resulted in a significantly enhanced PanIN outgrowth and progression (increased PanIN area and percentage of high-grade PanIN2/3 lesions) (Figure 7B–7D). Epithelial proliferation (Ki67 staining), ERK activation (pERK

staining) and Dclk1$^+$ cells were all significantly increased in Tff2 cell-ablated animals (Figure 7B, 7E, and S7G–I), suggesting that loss of Tff2$^+$ cells promoted pancreatic growth and preneoplasia.

While no significant inflammatory infiltrates were observed following Tff2+ cell ablation (Figure S7F), we further excluded any confounding DT-associated inflammation through dexamethasone treatment, an anti-inflammatory drug known to reduce pancreatic tumorigenesis in inflammation-induced tumor model.[50] As predicted, dexamethasone treatment did not impact tumorigenesis (both PanIN area and grade), suggesting that the inflammatory impact caused by Tff2$^+$ cell ablation is minimal (Figure S7K–S7M).

As we observed a significant increase in Dclk1 immunostaining in PanINs following Tff2$^+$ cell ablation, we next investigated the possible effect on quiescent Dclk1$^+$ FPs. We generated two sets of double *Cre-ER^{T2}* crosses, *Dclk1-CreER^{T2}; Tff2-DTR-CreER^{T2}; R26-tdTomato* mice and *Dclk1-CreER^{T2}; Tff2-DTR-CreER^{T2}; LSL-Kras$^{G12D/+}$; R26-tdTomato* mice. Indeed, ablation of Tff2$^+$ cells led to activation and lineage expansion of Dclk1$^+$ cells in both the ductal and acinar compartment (Figure 7F and 7G). A similar robust expansion of PanIN progression was seen in Dclk1$^+$ cells after Tff2$^+$ cell ablation in the *Kras$^{G12D/+}$* mice (Figure 7H), indicating that Tff2$^+$ TAPs restrict the activation of Dclk1$^+$ FP cells.

To further support a suppressive role for Tff2$^+$ cells and to test the functional significance of secreted TFF2 peptide, we overexpressed mouse Tff2 via adenoviral delivery of TFF2 (**Ad-Tff2**)51in DT-ablated *MTK* mice. Elevated serum Tff2 level post-adenoviral infection was confirmed by ELISA (data not shown). Interestinglly, treatment with Ad-Tff2 led to a marked reduction in PanIN area and proportion of PanIN2/3 lesions ($P<0.05$, Figure 7I–7L).

Taken together, these data define a suppressive role of Tff2$^+$ TAPs in oncogene-driven pancreatic tumorigenesis, which is partially through secretion of TFF2 peptides, thus preventing activation of FP cells.

DISCUSSION

Pancreatic acinar cells have been proposed to maintain the normal epithelium as well as serve as the origin of pancreatic adenocarcinoma.[19,52,53] Using a combination of genetic lineage tracing and single-cell sequencing approaches, we have defined a unique Tff2-labeled progenitor population that comprises a subset of acinar cells. These Tff2$^+$ progenitors show active proliferation, limited longevity and the ability to contribute to tissue homeostasis by giving rise to more differentiated cell types, consistent with a “transit amplifying progenitor” (TAP); however, they are also notable for their lack of regenerative potential following tissue injury. Importantly, these Tff2$^+$ cells are more resistant to mutant Kras transformation, and in fact appear to suppress the activation of FPs and pancreatic tumorigenesis. Nevertheless, in the context of pancreatitis or severe pancreatic injury, Kras mutant Tff2$^+$ cells survive and can interconvert into pancreatic CSCs, thus contributing to pancreatic tumorigenesis.

Active proliferation distinguishes Tff2$^+$ TAP cells from the Dclk1$^+$ or Bmi1$^+$ acinar progenitors, as well as from most acinar cells. Dclk1$^+$ cells remain largely quiescent in

normal homeostasis[9], while Bmil1$^+$ cells expand slowly but achieve a steady plateau at 60 days.[7] However, while Tff2+ cells expand from single-cell clones to clusters of cells, they lack long-term self-renewal, as their expansion peaks at 6 months followed by a gradual decline with a gradual loss of single clones. This contrasts with FP cells such as Dclk1$^+$ cells that continue to expand up to 18 months.[9] While scRNA-seq data suggest some heterogeneity among Tff2$^+$ cells, a significant portion of the Tff2 labeled cells (cluster 0) represent a less differentiated population, with high entropy scores and enrichment of Wnt/Notch/TGF-beta signaling pathways, and are strong candidates for the active progenitor cells.

Another distinct feature of the Tff2$^+$ population is its susceptibility to injury. Bmi1$^+$ acinar cells survive and self-renew following injury[7], and Dclk1$^+$ or Stmn$^+$ cells are immediately or transiently activated and participate substantially in pancreatic regeneration.[8,9] In contrast, caerulein-induced pancreatitis and PDL lead to severe and rapid depopulation of Tff2$^+$ cells. Acinar to ductal metaplasia is a transient state associated with pancreatic exocrine regeneration, but lineage tracing studies show that the majority of the pre-existing Tff2$^+$ cells disappear in various injury models rather than converting to regenerative population or ADM. This is consistent with reported data showing a lack of Tff2 expression in the injured acinar in human chronic pancreatitis.[54] Therefore, while Tff2$^+$ TAPs contribute to normal acinar homeostasis, other FPs mediate repair following injury and eventually regenerate the Tff2$^+$ TAPs (Figure 7M) and likely contribute to ADM. Dclk1+ acinar cells are highly resistant to caerulein pancreatitis and other types of injury[9], and such resistance to caerulein-induced injury has also been shown for Tert$^+$ facultative progenitors.[10] Following cerulein injury, newly-replenished/formed Tff2 cells do emerge from FP such as Dclk1$^+$ cells, and there is dynamic expansion of Tff2$^+$ cells of more than 5-fold, contributing to regeneration of up to 15% of the acinar pancreatic. This “2-progenitor cell” model (Figure 7M) as we proposed is similar to that proposed for organs such as the lung and epidermis[15]; while active progenitor cells are crucial for homeostasis, more quiescent progenitors/stem cells are more “dispensable” under normal conditions but become activated and mediate tissue repair.[55,56]

Among all the adult pancreatic cell types, acinar cells maintain a higher susceptibility to mutant Kras transformation. However, within the acinar compartment, oncogenic Kras activation may favor transformation of some but not all acinar subpopulations. Indeed, while activation of oncogenic Kras under the Mist1- or Elastase-CreER^{T2} promoter leads to extensive PanIN formation within 2 months[57], oncogenic Kras activation from the Elastase-tTA; TetO-Cre promoter results in virtually no PanIN formation at one year.[58] The higher rates of Kras transformation seen with Mist1- or Elastase-CreER^{T2} could be due in part to the higher Cre efficiency, the broader acinar coverage, or possibly the haploinsufficiency of the Mist1-CreER^{T2} knock-in allele.[59,60] In addition, differences in the type of mutant Kras used may also result in differential levels of oncogenic transformation.[47] Nevertheless, acinar cells labeled by the Tff2 promoter appear to be much more resistant to the Kras^{G12D} as compared to Mist1-, Elastase-, Tert- or Dclk1-CreER^{T2} labeled cells (Supplementary Table 1). Even when aged for up to 18 months or crossed with *LSL-Trp53$^{+/R172H}$* allele, the *Tff2-CreER^{T2}; LSL-Kras$^{G12D/+}$* mice did not progress to PDAC. However, following caerulein-induced pancreatitis, the limited Kras-mutant Tff2$^+$ acinar population, comprising

only 2% the acinus, was able to give rise to ADM and initiate PDAC more efficiently than cells traced by Elastase-CreER^{T2} or proCPACreER^{T2} (no PDAC initiation, Supplementary Table 1).

Tissue injury and pancreatitis have been strongly linked to PDAC initiation. Mechanistically, in the experimental rodent models, the promotional effects of the cholecystokinin analog caerulein in PDAC initiation have been attributed to activation of the EGFR signaling pathway[61,62] and Stat3[63], and inhibition of Kras-induced senescence.[64] Another possibility is the activation by caerulein of Kras-mutated progenitors, leading to transition to a CSC-like phenotype.[65] In addition, recent studies suggest that inflammation associated with caerulein-induced pancreatitis leads in facultative acinar progenitors (such as Dclk1$^+$ cells) to epigenetic reprgramming that can be maintained in the absence of mutant Kras signaling and primes acinar cells to transformation.[48] In this study, we demonstrated that Tff2$^+$ TAPs behave quite differently, are largely lost after acute pancreatitis and thus likely cannot become reprogrammed after pancreatitis (Figure S5I and S5J). However, oncogenic Kras signaling confers an *in vivo* survival benefit to Tff2$^+$ TAPs against injury-induced cell loss, thus allowing them to convert to a CSC state in the setting of pancreatitis. Blockade of the MEK pathway downstream of Kras signaling was able to abrogate this survival advantage, thus reducing interconversion towards a CSC state, pointing to the possible utility of MEK inhibitors in chemoprevention.

Surprisingly, ablation of Tff2$^+$ cells in the setting of a Kras transformed pancreatic acinar cells failed to slow PanIN progression, but instead led to more rapid PanIN progression. Thus, consistent with earlier observations, Tff2-expressing progenitors are suppressor cells that at baseline inhibit tumorigenesis of the gastrointestinal tract[27], particularly the development of pancreatic cancer.[28] Under normal conditions, ablation of Tff2$^+$ cells results in significant tissue atrophy and fatty metaplasia but this is eventually recoverable, with the replacement of lost Tff2$^+$ cells, presumably from FPs. In contrast, ablation of Tff2$^+$ cells in the setting of broad Kras^{G12D} activation in the acinar population results in massive and persistent infiltration of adipose tissues, with rapid progression to advanced PanINs. Presumably, in the presence of mutant Kras^{G12D}, FPs cannot replace or regenerate the normal acinar compartment but instead give rise to PanIN lesions. Our data suggest that that the presence of Tff2$^+$ TAPs helps to maintain the quiescence of FPs such as Dclk1$^+$ acinar cells, and indeed ablation of Tff2$^+$ cells leads to more activation and tracing from Dclk1$^+$ FP cells (Figure 7G–7H). Some of this suppression is mediated directly through secretion of Tff2 peptide, as delievery of Tff2 via adenovirus indeed suppressed tumorigenesis. Thus, in our “2-progenitor model”, the Tff2$^+$ TAP cells, highly susceptible to injury, serve as monitors for injurious stimuli, with the loss of Tff2+ cells representing a key trigger for regeneration. Overall, the findings suggest that one mechanism by which pancreatitis promotes Kras-dependent PDAC is through elimination of the “suppressive” Tff2$^+$ acinar progenitors, which then allows for the activation of Kras-susceptible FPs.

In summary, Tff2 defines a progenitor population with much less longevity than Dclk1 progenitors, and unlike facultative progenitors contributes to pancreatic homeostasis. Tff2$^+$ cells are dispensable for tissue regeneration and resistant to Kras transformation but can readily transition to CSCs with Kras mutation and acute pancreatitis. While much attention

has focused on regenerative progenitors, our data suggest that active progenitor cells that do not normally participate in regeneration, such as Tff2^{+} TAPs, can still contribute to Kras-driven PDAC progression in the context of pancreatitis. Finally, Tff2^{+} TAPs at baseline are strongly protective of tumorigenesis, as loss of this population leads to marked acceleration of PDAC. The TAPs may in fact serve as an important signal that maintains the quiescence of FPs, a protective mechanism to reduce the proliferative activity of the regenerative progenitors that are more susceptible to carcinogenic exposure.

Limitations of the Study:

The BAC transgenic constructs usually do not lineage trace every cell that expresses the mRNAs and therefore the Tff2 inducible Cre line is mosaic. In addition, the relationship between embryonic and adult Tff2 Cre lines were not investigated in this study.

STAR★Methods

RESOURCE AVAILABILITY

Lead contact—Requests for resources and reagents should be directed to and will be fulfilled by the Lead Contact, Timothy C. Wang (tcw21@cumc.columbia.edu).

Materials Availability—Mouse lines generated in this study have been deposited to Jackson laboratory (see Key Resource Table) and requests should be directed to and will be fulfilled by the Lead Contact. This study did not generate new unique reagents.

Data and Code Availability

- The scRNA-seq dataset generated during this study is available at Gene Expression Omnibus and the accession number is listed in the key resources table.
- This paper does not report original code.
- Any additional information required to reanalyze the data reported in this paper is available from the lead contact upon request.

EXPERIMENTAL MODEL AND SUBJECT DETAILS

Mouse Models

Generation of Tff2-DTR-CreER^{T2} and Dclk1-DTR-ZsGreen transgenic mice: BAC recombination was performed using the DTR-CreER^{T2}-FrtNeoFrt or the DTR-ZsGreen-FrtNeoFrt cassette, respectively, a similar strategy as described previously[23]. Briefly, these cassettes were ligated into a p451 plasmid before generating a probe containing a 40-bp sequence homologous to the BAC sequence, respectively. The BAC clones (RP23-332C16 for Tff2 and RP23–283D6 for Dclk1) were isolated and transferred into SW105-competent cells. After verifying the correct sequence, the purified cassette carrying the 40-bp BAC homolog on both ends was electroporated into SW105 BAC-containing cells for Tff2 or Dclk1. Isolated, linearized BAC DNA and then microinjected into the pronucleus of fertilized CBA × C57BL/6J oocytes at the Columbia University Transgenic Animal

Core facility. Founders were identified and backcrossed to C57BL/6J mice for at least 8 generations.

Mouse Crosses: For lineage-tracing studies in homeostasis and injury, Tff2-DTR-CreER^{T2} mice were crossed to Rosa26-tdTomato, Rosa26-mTmG, or Rosa26-tdTomato; Dclk1-DTR-ZsGreen mice. Tff2-Cre mice were crossed to Rosa26-Rainbow2.1 or Rosa26-tdTomato mice. For tumorigenesis studies, Tff2-DTR-CreER^{T2} mice were crossed to LSL-Kras$^{G12D/+}$, LSL-Kras$^{LSL\text{-}G12D/+}$; R26-mTmG, Mist1-CreERT2, Mist1-CreERT2; LSL-Kras$^{G12D/+}$, Dclk1-CreERT2; Rosa26-tdTomato, or Dclk1-CreERT2; LSL-Kras$^{G12D/+}$; Rosa26-tdTomato. Elastase-CreERT2 mice were kindly gifted by Dr. Steven Konieczny (Purdue University) and crossed to LSL-Kras$^{G12D/+}$, Rosa26-tdTomato or Rosa26-mTmG. All animal experiments were conducted in compliance with the National Institute of Health guidelines for animal research and approved by the Institutional Animal Care and Use Committee of Columbia University. Mice were housed in a specific pathogen-free facility.

Orthotopic transplantation in immunodeficient mice: EpCAM^{+} cells were sorted from Tff2-DTR-CreER^{T2}; LSL-Kras$^{LSL\text{-}G12D/+}$ mice with or without caerulein treatment (at 8 weeks post-treatment). About 50,000 sorted cells were mixed with Matrigel containing ROCK inhibitor (Y-27632, stock at 10μM and use 1 μl per 50 uL Matrigel) and transplanted into the pancreas of NOD SCID mice (8–10 weeks old). At 10 weeks after orthotopic transplantation, the whole pancreas was harvested, prepared in FFPE sections (five levels per sample) and analyzed.

METHOD DETAILS

Tamoxifen induction of Cre recombination: For lineage-tracing experiments, unless specified, one dose of tamoxifen (MilliporeSigma, 6 mg dissolved in corn oil at 37°C) was administrated to a 6-week old mouse. Quantification of recombination of mGFP cells in *Tff2-DTR-CreER^{T2}; R26-mTmG* mice after one dose of TM (1x, 6 mg) or three doses of TM (3x, 6 mg each) showed no significant differences between these two TM regimens (Figure S4G–S4H). Therefore, TM (1x, 6 mg) was used for lineage tracing experiments. For tumorigenesis studies, three doses of tamoxifen (6 mg each dissolved in corn oil at 37°C) was administrated. In some experiments, two doses of tamoxifen (3mg each) was used.

Caerulein-induced pancreatitis/tissue injury: In some experiments, mice were subjected to seven hourly intraperitoneal (i.p.) injections of caerulein (50 μg/kg dissolved in saline) on two consecutive days. In caerulein-induced chronic injury model, mice were subjected to daily intraperitoneal injections of caerulein (50 μg/kg) for 25 days.

Diphtheria toxin-mediated cell ablation: In some experiments, mice were subjected to intraperitoneal injections of diphtheria toxin (Sigma-Aldrich) (10, 15, 20 ng/20g BW) or 12.5 μg/kg (EMD Millipore, old batch) dissolved in PBS) on two or three consecutive days.

***In vivo BrdU* labeling:** For *BrdU* labeling experiment, mice were subjected to one intraperitoneal (i.p.) injection of *BrdU* (1mg in 200 uL) followed by continuous treatment of *BrdU* in drinking water for one month.

Dexamethansone treatment: Mice were treated with seven daily injections (i.p.) of dexamethasone or vehicle (DMSO) as described[50].

Adenoviral delievery: Mice were administrated adenoviral Tff2 or vector virus (i.v.) on 2 days before TM and 14 days after TM as described[51].

Pharmacological inhibition of ERK/MEK signaling: For *in vivo* inhibition of ERK signaling, Trametinib (GSK1120212, Selleckchem) at 3 mg/kg BW was administrated by daily gavage for 5 days unless otherwise specified. Trametinib stock (10 mg/mL in DMSO) was diluted in corn oil prior to being given to the animals.

Surgical Procedures

Partial pancreatectomy (Ppx): Tff2-DTR-CreER^{T2}; R26-mTmG mice (8–9 weeks old) were anesthetized using isoflurane and Ppx was performed as described previously[9]. Briefly, following laparotomy, the pancreatic tail was exteriorized after mobilizing the spleen. The pancreas was dissected until the level of the portal vein. The main two main branches from the celiac artery and superior mesenteric artery were ligated using 8.0 S&T Microsurgical sutures. Then the left-sided part of the organ together with the spleen was resected by transection above the splenic-mesenteric confluence with scissors, resulting in the removal of more than 70% of the pancreas. The resection side was immediately sealed using a disposable cautery. After checking for the cessation of bleeding, abdominal muscles were closed using 5−0 vicryl sutures (Ethicon), and the skin was stapled using 9.0-mm staples (Reflex Skin Closure Systems). Carprofen in normal saline (2 mg/kg) was injected subcutaneously for analgesia before and after the surgery. Mice were analyzed 2 weeks postoperatively.

Pancreatic duct ligation (PDL): Tff2-DTR-CreER^{T2}; Rosa26-mTmG mice (8–9 weeks old) were anesthetized using isoflurane and PDL was performed as described previously[9]. Briefly, following laparotomy, the pancreatic tail was exteriorized after mobilizing the spleen. The pancreas was dissected until the level of the portal vein. The main pancreatic duct was identified and ligated using 8.0 S&T Microssurgical sutures. After checking for the cessation of bleeding, abdominal muscles were closed using 5–0 vicryl sutures (Ethicon), and the skin was stapled using 9.0-mm staples (Reflex Skin Closure Systems). Carprofen in normal saline (2 mg/kg) was injected subcutaneously for analgesia before and after the surgery. Mice were analyzed 2 weeks postoperatively.

Dissection of pancreatic tissues from mouse embryos: Timed-pregnant female mice at embryonic days (E) 11.5–12.5 and 15.5–16.5 were enthanized and embryos were collected as described http://www.jove.com/video/3979/. Pancreatic bud and tissue in genotyping positive embryos were fixed, ppared for frozen sections, and analyzed using immunostaining.

Sphere Cultures: For isolated or FASC-sorted single cells from adult mouse pancreas, 3D spheroid cultures were performed according to the protocol described previously[66] with slight modification. Briefly, pancreatic tissue was minced into small pieces (1–2 mm in size)

and digested in DMEM/F12 medium containing collagenase-V (1 mg/mL), BSA (10mg/mL) and DNase I (2 U/mL) at 37 C° for 20 min. After multiple washes in ice-cold Hank's balanced salt solution (HBSS) supplemented with 5% FBS, pancreatic tissue was collected and centrifuged at 500g. The pellet was re-suspended in HBSS + FBS and mechanically broken down through a syringe with a 22-gauge needle. After multiple washes, cells were filtered through a 40 μm cell strainer and then into a polystyrene tube with a cell-strainer cap. Single cells were counted and resuspended in Matrigel (Corning) at a density as described in the experiment. Organoids were cultured in DMEM (Gibco) medium containing B27 and N2 supplements (Gibco), 5% Nu-Serum IV (Corning), 100 μg/ml trypsin inhibitor, and 100ng/ml Cholera Toxin (Sigma-Aldrich) for 5–7 days before analysis. The culture medium was replaced every other day. Sphere number and diameter were measured using ImageJ software.

Histology, Immunohistochemistry, and Immunocytochemistry—Tissues were harvested and fixed with 10% neutral-buffered formalin (VWR) and embedded into paraffin blocks. For immunohistochemical staining, formalin-fixed, paraffin-embedded (FFPE) sections (4 μm) were deparaffinized in xylene and rehydrated in gradient ethanol. Antigen retrieval was performed by heating the slides in citrate buffer in a steamer for 40 min. Endogenous peroxidase was blocked by incubation with 3% hydrogen peroxide (Sigma) in PBS. Slides were rinsed, blocked with 10% serum and incubated with primary antibodies (anti- Ki-67, Dclk1, pERK) overnight at 4 °C. Subsequently, slides were incubated with secondary antibodies (diluted in 2% BSA) at RT for 45 min followed by peroxidase-conjugated avidin (Vector Laboratories) and 3,3'diaminobenzidine (Dako) as a chromogen. For pERK staining, SignalStain® Boost IHC Detection Reagent was used. Slides were counterstained with hematoxylin.

For immunofluorescent staining on frozen sections, tissues were fixed in 4% paraformaldehyde (Electron Microscopy Sciences) overnight, infiltrated by 30% sucrose and embedded in OCT compound (Tissue-Tek). Sections (5 μm) were blocked with a blocking buffer. Primary antibodies were applied for overnight staining. AlexaFluor secondary antibodies (Invitrogen) were used to reveal the staining. All slides were counterstained and mounted with VECTASHIELD mounting medium with DAPI (Vector Labs). Images were acquired with a Nikon Ti Eclipse inverted microscopes or an A1 laser scanning confocal attachment on an Eclipse Ti microscope stand (Nikon Instruments). For *BrdU* staining, sections were subjected to antigen retrieval by submersion in 10mM sodium citrate, 0.05% (v/v) Tween 20 (MilliporeSigma) in distilled water (pH6.0) in a steamer for 30 minutes prior to blocking buffer. For confetti imaging by confocal microscopy, spectral imaging was used for the acquisition of Dapi, CFP, GFP, YFP and RFP channels. For thick section analysis by confocal microscopy, a 50 μm section was used. Titration of amylase antibody was performed with a dilution ratio starting from 1:100 and a ratio of 1:1600 was used. For immunofluorescent imaging for quantifications, images from Dapi channel were taken for quantifying the total number of the cells in a specific field. Images are all composites of different channels unless otherwise stated.

Acinar-ductal cell isolation from the mouse pancreas—Acinar and ductal cell isolation protocol was developed and kindly shared by Drs. Rohit Chandwar and Steven Leach. Briefly, mouse pancreas was dissected, minced and digested in dissocation solution containing an enzyme cocktail, $CaCl_2$ and P188. After filtering and wash with FBS-containing buffer, single layer cells were stained and subjected to cell sorting (see below).

Flow Cytometry Analysis and Cell Sorting—Mouse pancreatic tissues were harvested, minced and digested as described in murine pancreatic spheres section. For cancer stem cell analysis, single cells were stained with EpCAM, TER119, CD45, CD44, CD24, CD133 antibodies. For cell sorting and sphere culture, cells were stained with EpCAM, TER119, and CD45. DAPI (4',6-Diamidino-2-Phenylindole, Dihydrochloride) was used to exclude dead cells. All FACS analyses an on LSRII or LSRFortessa instruments. Cell sorting was performed on a BD Influx cell sorter. For acinar cell and ductal fraction isolation, single cells from the whole pancreas were stained for acinar cells ($TER119^-CD45^-CD49f^+CD133^-$) and ductal cells ($TER119^-CD45^-CD49f^+CD133^+$). Sorted cell fractions were analyzed by RT-qPCR for enrichment (Figure S1A).

Quantitative RT-PCR (RT-qPCR)—For mouse pancreas samples that were stored in RNAlater stabilization solution (Ambion), total RNA was extracted using the NucleoSpin RNA kit (Macherey-Nagel). For FACS-sorted cells, total RNA was extracted using the RNeasy Micro Kit (Qiagen). First-strand complementary DNA was synthesized using the Superscript III cDNA Amplification System (Invitrogen) following the manufacturer's instructions. qPCR was performed using an ABI 7300 PCR system and the SYBR green or TaqMan assays (Applied Biosystems). The RT-qPCR primer sequences are listed in Table S2. $2^{-\Delta\Delta Ct}$ was used to calculate the ratio of the expression of the gene of interest to the housekeeping gene Gapdh. In some experiments, $2^{-\Delta Ct}$ was used to express gene expression changes.

Western Blotting—Tissues (50 mg) were homogenized in ice-cold RIPA lysis buffer. Debris was removed by centrifugation. The protein content of the supernatant was determined by the bicinchoninic acid (BCA) kit, and the cellular lysates were separated by 10% SDS-PAGE and transferred onto polyvinylidene fluoride (PVDF) membranes. After being blocked with 10% non-fat milk in TBS-T, the membranes were incubated with primary antibodies at 4°C overnight, followed by 1:1000 horseradish peroxidase (HRP)-conjugated secondary antibody (GE Healthcare Life Sciences) for 1 hr. Immunoreactive bands were visualized using an enhanced chemiluminescence kit (Amersham). Primary antibodies used are listed in the Key Resources Table.

Single-cell RNA Sequencing (sc-RNAseq)—sc-RNAseq was performed at the Columbia Single Cell Analysis Core and using the Chromium Single Cell 3′ Library V3 Kit according to manufacturer's instructions. Briefly, single-cell suspensions ($CD45^-TER119^-EpCAM^+RFP^+$) from FACS-sorted Tff2-DTR-CreERT2; Rosa26-tdTomato mice (pooled from 4 or 6 mice) were prepared and loaded into the Chromium instrument (10X Genomics), and the resulting barcoded cDNAs were used to construct two libraries. Before sequencing, single-cell cDNA libraries were quantified using the TapeStation 2200

(Agilent) and Qubit (Thermo Fisher Scientific). RNA-seq was performed on each library (approximately 200 million reads/sample) using a NovaSeq 6000 system (Illumina) and sequencing data were combined for analysis.

RNA *In Situ* Hybridization (RNAScope®)—RNA ISH for fixed frozen tissues was performed at the Columbia Human Immune Monitoring Core (HIMC) using the RNAscope™ LS Multiplex Fluorescent Assay Kit [Advanced Cell Diagnostics (ACD), Newark, CA, USA] with the autostainer Leica Bond Rx System. Mouse Tff2- specific RNA probes (RNAscope® LS 2.5 Probe- Mm-Tff2, 439538) were purchased from ACD. Ppib (positive control) and dapB (negative control) were used as controls.

Enzyme-Linked Immunosorbent Assay (ELISA)—ELISA of mouse Tff2 in FACS-sorted cells was performed according to the manufacturers' manual (MybioSource).

QUANTIFICATION AND STATISTICAL ANALYSIS

Quantification of recombination in Tff2-DTR-CreER^{T2}; Rosa26-mTmG mice: For lineage-tracing experiments, recombination was assessed using 8–10 randomly selected high power fields (40x). Recombined cells were counted with the CellCounter plugin in Fiji. The total cells in a field were enumerated by counting the number of DAPI positive nuclei using a macro function in Fiji. The percentage of recombination was calculated by the number of total recombined cells against the total cell numbers. To evaluate the expansion of recombined cells, recombined cells were classified as single clones and clusters of two or more cells (expanded clones). In these experiments, over 100 recombined cell groups were selected based on their respective morphology and grouped as mentioned above.

Morphometric analysis of mPanINs: Tff2-DTR-CreER^{T2}; LSL-Kras$^{G12D/+}$ mice with or without caerulein treatment were analyzed at 3, 6, 12 or 18 months after tamoxifen induction. For each mouse, level sections were analyzed and ten fields (40x) were randomly selected per level section. Morphometric analysis was done using ImageJ. Histological scoring was performed according to published criteria by board-certified gastrointestinal pathologists (A.C.I.) who were blinded as to sample identity. For scoring murine pancreatic intraepithelial neoplasia (PanIN), PanIN was scored based on the degree of cytological atypia and epithelial proliferation. Microinvasion was also identified in association with foci of small duct intraepithelial neoplasia. The majority of small duct intraepithelial neoplasia consists of flat neoplastic lesions: 1. mucinous epithelial lining with minimal cytological atypia (PanIN-1), 2. atypical epithelial lining with preserved nuclear polarity (PanIN-2) and 3. Intraductal epithelial proliferation filling and expanding small ducts, showing severe cytological atypia, loss of polarity, increased mitotic activity, nuclear enlargement with irregular contours and hyperchromasia (PanIN-3). Ten consecutive ductal areas were scored for small duct intraepithelial neoplasia. Nodular clusters of coalescing small ducts expanded by solid neoplastic epithelial proliferation were seen. These microcarcinomas showed foci of microinvasion and were also seen adjacent to larger poorly differentiated carcinomas. The number of microcarcinomas was assessed on full-face sections of the entire mouse pancreas.

Quantification of immunohistochemical staining: Ki67, Dclk1 and pERK positive cells were quantified in at least five high power fields from at least 6 mice per group using Fiji.

Singe-cell RNA Sequencing Analysis: Singe-cell RNA sequencing data were analyzed using the 10X CellRanger software (10x Genomics). Samples were combined using the Cell Ranger aggregate function. Gene-cell matrix was filtered to remove cells with less than 1000 transcripts and/or a high fraction of mitochondrial counts (>30%). From 922 sequenced cells, 194 cells were removed during our quality control. The gene expression profiles of the 728 high quality cells were normalized to CPM and z-score transformed for VIPER analysis. However, even if all these cells were FACS-sorted for Tff2, only 358 cells showed detectable levels of Tff2 transcripts. To exclude any possible results due to the technical noise that affects single cell sequencing[68], we focused our downstream analyses on the subset (358 cells) of Tff2-expressing cells. The gene-cell matrix was then normalized to count per million of reads (cpm). Normalized single-cell gene expression profiles were transformed to gene expression signature by z-score procedure and used to compute metacell profiles. Metacell profiles were used as input for ARACNe[67] to reverse engineering a regulatory network. Specifically, z-score expression signatures were used to identify for each individual cell the closest 10 cells based on the reciprocal enrichment analysis of the 200 most differentially expressed genes (100 most overexpressed and 100 most downregulated) as implemented in the viperSimilarity function of the VIPER package. A metacell profile was then generated for each cell by integrating the raw counts of the 10 closest cells (KNN approach) in the viperSimilarity space. Metacell profiles were normalized and used as input for ARACNe. ARACNe was run with 100 bootstrap iterations using 1824 transcription factors (genes annotated in gene ontology molecular function database, as GO:0003700, “transcription factor activity”, or as GO:0003677, “DNA binding”, and GO:0030528, “transcription regulator activity”, or as GO:00034677 and GO: 0045449, “regulation of transcription”) and 3477 signaling pathway-related genes (annotated in GO biological process database as GO:0007165 “signal transduction” and in GO cellular component database as GO:0005622, “intracellular”, or GO:0005886, “plasma membrane”). ARACNe was able to infer the regulons of 2774 regulatory proteins.

The single-cell regulatory network inferred by ARACNe and the gene expression signature were used to compute protein activity of the 354 cells expressing Tff2 using the Virtual Inference of Protein-activity by Enriched Regulon (VIPER) algorithm, a network-based algorithm for protein activity inference from gene expression data[39]. The VIPER algorithm uses the transcriptional target genes of a given regulatory protein (referred to as a regulon) as the reporter of its activity. Cluster analysis was performed using the Louvain algorithm as implemented in the Seurat package with the resolution parameter optimized by silhouette analysis which yielded a resolution value of 0.3. Protein activity markers for each cluster were identified by the “FindAllMarkers” function implemented in Seurat using the “roc” method. Differential gene expression analysis was performed using the Seurat package from raw counts of the 354 Tff2 expressing cells. Seurat was used to normalize and scale the data using the functions “NormalizeData” and “ScaleData”, respectively. The “FindAllMarkers” was used to identify the differentially expressed genes across the clusters

(previously identified on the VIPER inferred protein activity profiles) using the default method (Wilcoxon test).

Single-cell entropy analysis was performed using the SLICE algorithm[69] on the gene expression profiles. Functional clusters were computed by the "getEntropy" function on the correlation matrix generated on the z-score transformed gene expression profiles.

The pseudo trajectory analysis was inferred by the Monocle algorithm on the VIPER-inferred protein activity profiles.

Pathway and gene ontology: For the pathway analysis of the differential expression datasets for each of the clusters, Enrichr was used (See Key Resources Table).

Statistical Analysis: Statistical testing was performed using GraphPad Prism 7 software (GraphPad Software Inc.). For experiments with two groups, unless specified, the differences between the means were compared using the Student's *t*-test (two-tailed). For experiments with three or more groups, one-way or two-way ANOVA with post hoc Tukey's or Dunnett multiple comparisons were performed. Statistical significance was depicted as follows: *= $p < 0.05$, **= $p < 0.005$ and ***= $p < 0.0005$.

Supplementary Material

Refer to Web version on PubMed Central for supplementary material.

ACKNOWLEDGMENTS

This work was supported by NIH (R35CA210088) to T.C.W. T.T. and R.T. were supported by Uehara Memorial Foundation. N.F. and W.C. were supported by the National Natural Science Foundation of China (NO. 81700525 for N.F.) and (NO. 81602035 for W.C.). B.W.R. was supported by a German Research Foundation grant (DFG RE3440/1-1). M.M. was supported by a postdoctoral fellowship grant from the Mildred-Scheel-Stiftung, Germany (NO. 70111870). Y.H. was supported by the Project for Cancer Research and Therapeutic Evolution (P-CREATE) from the Japan Agency of Medical Research and Development (AMED). We thank Dr. Chyuan-Sheng Lin from Columbia Transgenic Mouse Shared Resource (TMSR) for generating transgenic mice (supported by NCI P30CA013696-40). We thank Drs. Caisheng Lu and Wei Wang from the CCTI Flow Cytometry Core (supported in part by the Office of the Director, NIH, under awards S10OD020056, S10RR027050, and P30CA013696). We thank Drs. Theresa Swayne and Laura Munteanu for confetti imaging assistance. Images were collected and analyzed at the Confocal and Specialized Microscopy Shared Resource at Columbia University, supported by NIH Grant P30 CA013696 (NCI). We thank Erin C Bush for her expertise in the single-cell sequencing experiment (supported through NIH/NCI Cancer Center Support Grant P30CA013696 for the Genomics and High Throughput Screening Shared Resource). This research was also supported by the Columbia Univesity Digestive and Liver Disease Research Center (CU-DLDRC) grant P30DK132710 and used the CU-DLDRC BioImaging Core. We thank Dr. Saito Yoshinobu for his technical expertise in supporting the adenoviral experiments and Dr. Yongchun Zhang for dissecting mouse embryos.

INCLUSION AND DIVERISTY

One or more of the authors of this paper self-identifies as an underrepresented ethnic minority in their field of research or within their geographical location. One or more of the authors of this paper self-identifies as a gender minority in their field of research.

References

1. Puri S, Folias AE, and Hebrok M (2015). Plasticity and dedifferentiation within the pancreas: development, homeostasis, and disease. Cell stem cell 16, 18–31. 10.1016/j.stem.2014.11.001. [PubMed: 25465113]
2. Puri S, and Hebrok M (2010). Cellular plasticity within the pancreas--lessons learned from development. Dev Cell 18, 342–356. 10.1016/j.devcel.2010.02.005. [PubMed: 20230744]
3. Kopp JL, Dubois CL, Schaffer AE, Hao E, Shih HP, Seymour PA, Ma J, and Sander M (2011). Sox9+ ductal cells are multipotent progenitors throughout development but do not produce new endocrine cells in the normal or injured adult pancreas. Development 138, 653–665. 10.1242/dev.056499. [PubMed: 21266405]
4. Kopinke D, Brailsford M, Shea JE, Leavitt R, Scaife CL, and Murtaugh LC (2011). Lineage tracing reveals the dynamic contribution of Hes1+ cells to the developing and adult pancreas. Development 138, 431–441. 10.1242/dev.053843. [PubMed: 21205788]
5. Lodestijn SC, van den Bosch T, Nijman LE, Moreno LF, Schlingemann S, Sheraton VM, van Neerven SM, Koning JJ, Vieira Braga FA, Paauw NJ, et al. (2021). Continuous clonal labeling reveals uniform progenitor potential in the adult exocrine pancreas. Cell stem cell 28, 2009–2019.e2004. 10.1016/j.stem.2021.07.004. [PubMed: 34358441]
6. Lodestijn SC, van Neerven SM, Vermeulen L, and Bijlsma MF (2021). Stem Cells in the Exocrine Pancreas during Homeostasis, Injury, and Cancer. Cancers 13. 10.3390/cancers13133295.
7. Sangiorgi E, and Capecchi MR (2009). Bmi1 lineage tracing identifies a selfrenewing pancreatic acinar cell subpopulation capable of maintaining pancreatic organ homeostasis. Proceedings of the National Academy of Sciences of the United States of America 106, 7101–7106. 10.1073/pnas.0902508106. [PubMed: 19372370]
8. Wollny D, Zhao S, Everlien I, Lun X, Brunken J, Brüne D, Ziebell F, Tabansky I, Weichert W, Marciniak-Czochra A, and Martin-Villalba A (2016). Single-Cell Analysis Uncovers Clonal Acinar Cell Heterogeneity in the Adult Pancreas. Dev Cell 39, 289–301. 10.1016/j.devcel.2016.10.002. [PubMed: 27923766]
9. Westphalen CB, Takemoto Y, Tanaka T, Macchini M, Jiang Z, Renz BW, Chen X, Ormanns S, Nagar K, Tailor Y, et al. (2016). Dclk1 Defines Quiescent Pancreatic Progenitors that Promote Injury-Induced Regeneration and Tumorigenesis. Cell stem cell 18, 441–455. 10.1016/j.stem.2016.03.016. [PubMed: 27058937]
10. Neuhofer P, Roake CM, Kim SJ, Lu RJ, West RB, Charville GW, and Artandi SE (2021). Acinar cell clonal expansion in pancreas homeostasis and carcinogenesis. Nature 597, 715–719. 10.1038/s41586-021-03916-2. [PubMed: 34526722]
11. Zhou Q, and Melton DA (2018). Pancreas regeneration. Nature 557, 351–358. 10.1038/s41586-018-0088-0. [PubMed: 29769672]
12. Murtaugh LC, and Keefe MD (2015). Regeneration and repair of the exocrine pancreas. Annu Rev Physiol 77, 229–249. 10.1146/annurev-physiol-021014-071727. [PubMed: 25386992]
13. Hsu YC, Li L, and Fuchs E (2014). Transit-amplifying cells orchestrate stem cell activity and tissue regeneration. Cell 157, 935–949. 10.1016/j.cell.2014.02.057. [PubMed: 24813615]
14. Muraro MJ, Dharmadhikari G, Grün D, Groen N, Dielen T, Jansen E, van Gurp L, Engelse MA, Carlotti F, de Koning EJ, and van Oudenaarden A (2016). A Single-Cell Transcriptome Atlas of the Human Pancreas. Cell Syst 3, 385–394.e383. 10.1016/j.cels.2016.09.002. [PubMed: 27693023]
15. Jiang Z, White RA, and Wang TC (2020). Adult Pancreatic Acinar Progenitor-like Populations in Regeneration and Cancer. Trends Mol Med 26, 758–767. 10.1016/j.molmed.2020.04.003. [PubMed: 32362534]
16. Young RC (1993). Cancer prevention. Archives of otolaryngology--head & neck surgery 119, 732–734. 10.1001/archotol.1993.01880190028005. [PubMed: 8318202]
17. Sánchez-Danés A, Hannezo E, Larsimont JC, Liagre M, Youssef KK, Simons BD, and Blanpain C (2016). Defining the clonal dynamics leading to mouse skin tumour initiation. Nature 536, 298–303. 10.1038/nature19069. [PubMed: 27459053]

18. di Magliano MP, and Logsdon CD (2013). Roles for KRAS in pancreatic tumor development and progression. Gastroenterology 144, 1220–1229. 10.1053/j.gastro.2013.01.071. [PubMed: 23622131]
19. Kopp JL, von Figura G, Mayes E, Liu FF, Dubois CL, Morris J.P.t., Pan FC, Akiyama H, Wright CV, Jensen K, et al. (2012). Identification of Sox9-dependent acinar-to-ductal reprogramming as the principal mechanism for initiation of pancreatic ductal adenocarcinoma. Cancer cell 22, 737–750. 10.1016/j.ccr.2012.10.025. [PubMed: 23201164]
20. Brembeck FH, Schreiber FS, Deramaudt TB, Craig L, Rhoades B, Swain G, Grippo P, Stoffers DA, Silberg DG, and Rustgi AK (2003). The mutant K-ras oncogene causes pancreatic periductal lymphocytic infiltration and gastric mucous neck cell hyperplasia in transgenic mice. Cancer research 63, 2005–2009. [PubMed: 12727809]
21. Font-Burgada J, Shalapour S, Ramaswamy S, Hsueh B, Rossell D, Umemura A, Taniguchi K, Nakagawa H, Valasek MA, Ye L, et al. (2015). Hybrid Periportal Hepatocytes Regenerate the Injured Liver without Giving Rise to Cancer. Cell 162, 766–779. 10.1016/j.cell.2015.07.026. [PubMed: 26276631]
22. Kuraishy A, Karin M, and Grivennikov SI (2011). Tumor promotion via injury- and death-induced inflammation. Immunity 35, 467–477. 10.1016/j.immuni.2011.09.006. [PubMed: 22035839]
23. Quante M, Marrache F, Goldenring JR, and Wang TC (2010). TFF2 mRNA transcript expression marks a gland progenitor cell of the gastric oxyntic mucosa. Gastroenterology 139, 2018–2027 e2012. 10.1053/j.gastro.2010.08.003. [PubMed: 20708616]
24. Kjellev S (2009). The trefoil factor family - small peptides with multiple functionalities. Cellular and molecular life sciences : CMLS 66, 1350–1369. 10.1007/s00018-008-8646-5. [PubMed: 19099184]
25. Hirata K, Kodama S, Nakano Y, Minaki-Nakagawa Y, Aoyama Y, Sakikubo M, Goto T, Yoshida M, Masui T, Yamamoto T, et al. (2019). Exocrine tissue-driven TFF2 prevents apoptotic cell death of endocrine lineage during pancreas organogenesis. Sci Rep 9, 1636. 10.1038/s41598-018-38062-9. [PubMed: 30733468]
26. Fox JG, Rogers AB, Whary MT, Ge Z, Ohtani M, Jones EK, and Wang TC (2007). Accelerated progression of gastritis to dysplasia in the pyloric antrum of TFF2 −/− C57BL6 x Sv129 Helicobacter pylori-infected mice. The American journal of pathology 171, 1520–1528. 10.2353/ajpath.2007.070249. [PubMed: 17982128]
27. Dubeykovskaya Z, Si Y, Chen X, Worthley DL, Renz BW, Urbanska AM, Hayakawa Y, Xu T, Westphalen CB, Dubeykovskiy A, et al. (2016). Neural innervation stimulates splenic TFF2 to arrest myeloid cell expansion and cancer. Nat Commun 7, 10517. 10.1038/ncomms10517. [PubMed: 26841680]
28. Yamaguchi J, Mino-Kenudson M, Liss AS, Chowdhury S, Wang TC, Fernandez-Del Castillo C, Lillemoe KD, Warshaw AL, and Thayer SP (2016). Loss of Trefoil Factor 2 From Pancreatic Duct Glands Promotes Formation of Intraductal Papillary Mucinous Neoplasms in Mice. Gastroenterology 151, 1232–1244 e1210. 10.1053/j.gastro.2016.07.045. [PubMed: 27523981]
29. Jorgensen KH, Thim L, and Jacobsen HE (1982). Pancreatic spasmolytic polypeptide (PSP): I. Preparation and initial chemical characterization of a new polypeptide from porcine pancreas. Regulatory peptides 3, 207–219. 10.1016/0167-0115(82)90126-4. [PubMed: 6896240]
30. Rasmussen TN, Raaberg L, Poulsen SS, Thim L, and Holst JJ (1992). Immunohistochemical localization of pancreatic spasmolytic polypeptide (PSP) in the pig. Histochemistry 98, 113–119. 10.1007/bf00717002. [PubMed: 1429019]
31. Terris B, Blaveri E, Crnogorac-Jurcevic T, Jones M, Missiaglia E, Ruszniewski P, Sauvanet A, and Lemoine NR (2002). Characterization of gene expression profiles in intraductal papillary-mucinous tumors of the pancreas. The American journal of pathology 160, 1745–1754. 10.1016/s0002-9440(10)61121-2. [PubMed: 12000726]
32. Ohshio G, Suwa H, Kawaguchi Y, Imamura M, Yamaoka Y, Yamabe H, Matsumoto M, Yoshioka H, Hashimoto Y, and Takeda H (2000). Differential expression of human spasmolytic polypeptide (trefoil factor family-2) in pancreatic carcinomas, ampullary carcinomas, and mucin-producing tumors of the pancreas. Dig Dis Sci 45, 659–664. 10.1023/a:1005471005289. [PubMed: 10759231]

33. Pin CL, Rukstalis JM, Johnson C, and Konieczny SF (2001). The bHLH transcription factor Mist1 is required to maintain exocrine pancreas cell organization and acinar cell identity. The Journal of cell biology 155, 519–530. 10.1083/jcb.200105060. [PubMed: 11696558]
34. Lynn FC, Smith SB, Wilson ME, Yang KY, Nekrep N, and German MS (2007). Sox9 coordinates a transcriptional network in pancreatic progenitor cells. Proceedings of the National Academy of Sciences of the United States of America 104, 10500–10505. 10.1073/pnas.0704054104. [PubMed: 17563382]
35. Kong B, Michalski CW, Erkan M, Friess H, and Kleeff J (2011). From tissue turnover to the cell of origin for pancreatic cancer. Nature reviews. Gastroenterology & hepatology 8, 467–472. 10.1038/nrgastro.2011.114. [PubMed: 21750515]
36. Carro MS, Lim WK, Alvarez MJ, Bollo RJ, Zhao X, Snyder EY, Sulman EP, Anne SL, Doetsch F, Colman H, et al. (2010). The transcriptional network for mesenchymal transformation of brain tumours. Nature 463, 318–325. 10.1038/nature08712. [PubMed: 20032975]
37. Basso K, Margolin AA, Stolovitzky G, Klein U, Dalla-Favera R, and Califano A (2005). Reverse engineering of regulatory networks in human B cells. Nat Genet 37, 382–390. 10.1038/ng1532. [PubMed: 15778709]
38. Margolin AA, Nemenman I, Basso K, Wiggins C, Stolovitzky G, Dalla Favera R, and Califano A (2006). ARACNE: an algorithm for the reconstruction of gene regulatory networks in a mammalian cellular context. BMC Bioinformatics 7 Suppl 1, S7. 10.1186/1471-2105-7-s1-s7.
39. Alvarez MJ, Shen Y, Giorgi FM, Lachmann A, Ding BB, Ye BH, and Califano A (2016). Functional characterization of somatic mutations in cancer using network-based inference of protein activity. Nat Genet 48, 838–847. 10.1038/ng.3593. [PubMed: 27322546]
40. Obradovic A, Chowdhury N, Haake SM, Ager C, Wang V, Vlahos L, Guo XV, Aggen DH, Rathmell WK, Jonasch E, et al. (2021). Single-cell protein activity analysis identifies recurrence-associated renal tumor macrophages. Cell 184, 2988–3005.e2916. 10.1016/j.cell.2021.04.038. [PubMed: 34019793]
41. Chen EY, Tan CM, Kou Y, Duan Q, Wang Z, Meirelles GV, Clark NR, and Ma'ayan A (2013). Enrichr: interactive and collaborative HTML5 gene list enrichment analysis tool. BMC Bioinformatics 14, 128. 10.1186/1471-2105-14-128. [PubMed: 23586463]
42. Yu X, Zou J, Ye Z, Hammond H, Chen G, Tokunaga A, Mali P, Li YM, Civin C, Gaiano N, and Cheng L (2008). Notch signaling activation in human embryonic stem cells is required for embryonic, but not trophoblastic, lineage commitment. Cell stem cell 2, 461–471. 10.1016/j.stem.2008.03.001. [PubMed: 18462696]
43. Yang H, Lee CJ, Zhang L, Sans MD, and Simeone DM (2008). Regulation of transforming growth factor beta-induced responses by protein kinase A in pancreatic acinar cells. American journal of physiology. Gastrointestinal and liver physiology 295, G170–g178. 10.1152/ajpgi.00492.2007. [PubMed: 18467503]
44. Nusse R (2008). Wnt signaling and stem cell control. Cell Res 18, 523–527. 10.1038/cr.2008.47. [PubMed: 18392048]
45. Barker N (2014). Adult intestinal stem cells: critical drivers of epithelial homeostasis and regeneration. Nature reviews. Molecular cell biology 15, 19–33. 10.1038/nrm3721. [PubMed: 24326621]
46. Moon H, Zhu J, Donahue LR, Choi E, and White AC (2019). Krt5(+)/Krt15(+) foregut basal progenitors give rise to cyclooxygenase-2-dependent tumours in response to gastric acid stress. Nat Commun 10, 2225. 10.1038/s41467-019-10194-0. [PubMed: 31110179]
47. Gidekel Friedlander SY, Chu GC, Snyder EL, Girnius N, Dibelius G, Crowley D, Vasile E, DePinho RA, and Jacks T (2009). Context-dependent transformation of adult pancreatic cells by oncogenic K-Ras. Cancer cell 16, 379–389. 10.1016/j.ccr.2009.09.027. [PubMed: 19878870]
48. Del Poggetto E, Ho IL, Balestrieri C, Yen EY, Zhang S, Citron F, Shah R, Corti D, Diaferia GR, Li CY, et al. (2021). Epithelial memory of inflammation limits tissue damage while promoting pancreatic tumorigenesis. Science 373, eabj0486. 10.1126/science.abj0486. [PubMed: 34529467]
49. Halbrook CJ, Wen HJ, Ruggeri JM, Takeuchi KK, Zhang Y, di Magliano MP, and Crawford HC (2017). Mitogen-activated Protein Kinase Kinase Activity Maintains Acinar-to-Ductal Metaplasia

and Is Required for Organ Regeneration in Pancreatitis. Cell Mol Gastroenterol Hepatol 3, 99–118. 10.1016/j.jcmgh.2016.09.009. [PubMed: 28090569]

50. Rhim AD, Mirek ET, Aiello NM, Maitra A, Bailey JM, McAllister F, Reichert M, Beatty GL, Rustgi AK, Vonderheide RH, et al. (2012). EMT and dissemination precede pancreatic tumor formation. Cell 148, 349–361. 10.1016/j.cell.2011.11.025. [PubMed: 22265420]
51. Dubeykovskaya ZA, Duddempudi PK, Deng H, Valenti G, Cuti KL, Nagar K, Tailor Y, Guha C, Kitajewski J, and Wang TC (2019). Therapeutic potential of adenovirus-mediated TFF2-CTP-Flag peptide for treatment of colorectal cancer. Cancer Gene Ther 26, 48–57. 10.1038/s41417-018-0036-z. [PubMed: 30042499]
52. Giroux V, Lento AA, Islam M, Pitarresi JR, Kharbanda A, Hamilton KE, Whelan KA, Long A, Rhoades B, Tang Q, et al. (2017). Long-lived keratin 15+ esophageal progenitor cells contribute to homeostasis and regeneration. The Journal of clinical investigation 127, 2378–2391. 10.1172/jci88941. [PubMed: 28481227]
53. Desai BM, Oliver-Krasinski J, De Leon DD, Farzad C, Hong N, Leach SD, and Stoffers DA (2007). Preexisting pancreatic acinar cells contribute to acinar cell, but not islet beta cell, regeneration. The Journal of clinical investigation 117, 971–977. 10.1172/jci29988. [PubMed: 17404620]
54. Ma Z, Lytle NK, Chen B, Jyotsana N, Novak SW, Cho CJ, Caplan L, Ben-Levy O, Neininger AC, Burnette DT, et al. (2022). Single-Cell Transcriptomics Reveals a Conserved Metaplasia Program in Pancreatic Injury. Gastroenterology 162, 604–620.e620. 10.1053/j.gastro.2021.10.027. [PubMed: 34695382]
55. Giangreco A, Arwert EN, Rosewell IR, Snyder J, Watt FM, and Stripp BR (2009). Stem cells are dispensable for lung homeostasis but restore airways after injury. Proceedings of the National Academy of Sciences of the United States of America 106, 9286–9291. 10.1073/pnas.0900668106. [PubMed: 19478060]
56. Yan X, and Owens DM (2008). The skin: a home to multiple classes of epithelial progenitor cells. Stem Cell Rev 4, 113–118. 10.1007/s12015-008-9022-4. [PubMed: 18491239]
57. Habbe N, Shi G, Meguid RA, Fendrich V, Esni F, Chen H, Feldmann G, Stoffers DA, Konieczny SF, Leach SD, and Maitra A (2008). Spontaneous induction of murine pancreatic intraepithelial neoplasia (mPanIN) by acinar cell targeting of oncogenic Kras in adult mice. Proceedings of the National Academy of Sciences of the United States of America 105, 18913–18918. 10.1073/pnas.0810097105. [PubMed: 19028870]
58. Guerra C, Schuhmacher AJ, Cañamero M, Grippo PJ, Verdaguer L, Pérez-Gallego L, Dubus P, Sandgren EP, and Barbacid M (2007). Chronic pancreatitis is essential for induction of pancreatic ductal adenocarcinoma by K-Ras oncogenes in adult mice. Cancer cell 11, 291–302. 10.1016/j.ccr.2007.01.012. [PubMed: 17349585]
59. Tuveson DA, Zhu L, Gopinathan A, Willis NA, Kachatrian L, Grochow R, Pin CL, Mitin NY, Taparowsky EJ, Gimotty PA, et al. (2006). Mist1-KrasG12D knock-in mice develop mixed differentiation metastatic exocrine pancreatic carcinoma and hepatocellular carcinoma. Cancer research 66, 242–247. 10.1158/0008-5472.CAN-05-2305. [PubMed: 16397237]
60. Hess DA, Humphrey SE, Ishibashi J, Damsz B, Lee AH, Glimcher LH, and Konieczny SF (2011). Extensive pancreas regeneration following acinar-specific disruption of Xbp1 in mice. Gastroenterology 141, 1463–1472. 10.1053/j.gastro.2011.06.045. [PubMed: 21704586]
61. Ardito CM, Grüner BM, Takeuchi KK, Lubeseder-Martellato C, Teichmann N, Mazur PK, Delgiorno KE, Carpenter ES, Halbrook CJ, Hall JC, et al. (2012). EGF receptor is required for KRAS-induced pancreatic tumorigenesis. Cancer cell 22, 304–317. 10.1016/j.ccr.2012.07.024. [PubMed: 22975374]
62. Navas C, Hernández-Porras I, Schuhmacher AJ, Sibilia M, Guerra C, and Barbacid M (2012). EGF receptor signaling is essential for k-ras oncogene-driven pancreatic ductal adenocarcinoma. Cancer cell 22, 318–330. 10.1016/j.ccr.2012.08.001. [PubMed: 22975375]
63. Fukuda A, Wang SC, Morris J.P.t., Folias AE, Liou A, Kim GE, Akira S, Boucher KM, Firpo MA, Mulvihill SJ, and Hebrok M (2011). Stat3 and MMP7 contribute to pancreatic ductal adenocarcinoma initiation and progression. Cancer cell 19, 441–455. 10.1016/j.ccr.2011.03.002. [PubMed: 21481787]

64. Guerra C, Collado M, Navas C, Schuhmacher AJ, Hernández-Porras I, Cañamero M, Rodriguez-Justo M, Serrano M, and Barbacid M (2011). Pancreatitis-induced inflammation contributes to pancreatic cancer by inhibiting oncogene-induced senescence. Cancer cell 19, 728–739. 10.1016/j.ccr.2011.05.011. [PubMed: 21665147]

65. Grivennikov SI, Greten FR, and Karin M (2010). Immunity, inflammation, and cancer. Cell 140, 883–899. 10.1016/j.cell.2010.01.025. [PubMed: 20303878]

66. Shi G, Zhu L, Sun Y, Bettencourt R, Damsz B, Hruban RH, and Konieczny SF (2009). Loss of the acinar-restricted transcription factor Mist1 accelerates Kras-induced pancreatic intraepithelial neoplasia. Gastroenterology 136, 1368–1378. 10.1053/j.gastro.2008.12.066. [PubMed: 19249398]

67. Hayakawa Y, Sakitani K, Konishi M, Asfaha S, Niikura R, Tomita H, Renz BW, Tailor Y, Macchini M, Middelhoff M, et al. (2017). Nerve Growth Factor Promotes Gastric Tumorigenesis through Aberrant Cholinergic Signaling. Cancer cell 31, 21–34. 10.1016/j.ccell.2016.11.005. [PubMed: 27989802]

68. Team, R.C. (2022). R: A Language and Environment for Statistical Computing. R Foundation for Statistical Computing.

69. Lachmann A, Giorgi FM, Lopez G, and Califano A (2016). ARACNe-AP: gene network reverse engineering through adaptive partitioning inference of mutual information. Bioinformatics 32, 2233–2235. 10.1093/bioinformatics/btw216. [PubMed: 27153652]

70. Hao Y, Hao S, Andersen-Nissen E, Mauck WM 3rd, Zheng S, Butler A, Lee MJ, Wilk AJ, Darby C, Zager M, et al. (2021). Integrated analysis of multimodal single-cell data. Cell 184, 3573–3587 e3529. 10.1016/j.cell.2021.04.048. [PubMed: 34062119]

71. and, M.M.a.P.R.a.A.S., and Hornik M.H.a.K. (2022). cluster: Cluster Analysis Basics and Extensions.

72. Gu Z, Eils R, and Schlesner M (2016). Complex heatmaps reveal patterns and correlations in multidimensional genomic data. Bioinformatics 32, 2847–2849. 10.1093/bioinformatics/btw313. [PubMed: 27207943]

73. Xie Z, Bailey A, Kuleshov MV, Clarke DJB, Evangelista JE, Jenkins SL, Lachmann A, Wojciechowicz ML, Kropiwnicki E, Jagodnik KM, et al. (2021). Gene Set Knowledge Discovery with Enrichr. Current protocols 1, e90. 10.1002/cpz1.90. [PubMed: 33780170]

74. Trapnell C, Cacchiarelli D, Grimsby J, Pokharel P, Li S, Morse M, Lennon NJ, Livak KJ, Mikkelsen TS, and Rinn JL (2014). The dynamics and regulators of cell fate decisions are revealed by pseudotemporal ordering of single cells. Nat Biotechnol 32, 381–386. 10.1038/nbt.2859. [PubMed: 24658644]

75. Wickham H (2016). ggplot2: Elegant Graphics for Data Analysis (Springer-Verlag New York).

76. Guo M, Bao EL, Wagner M, Whitsett JA, and Xu Y (2017). SLICE: determining cell differentiation and lineage based on single cell entropy. Nucleic Acids Res 45, e54. 10.1093/nar/gkw1278. [PubMed: 27998929]

77. Reichert M, Takano S, Heeg S, Bakir B, Botta GP, and Rustgi AK (2013). Isolation, culture and genetic manipulation of mouse pancreatic ductal cells. Nat Protoc 8, 1354–1365. 10.1038/nprot.2013.079. [PubMed: 23787893]

78. Luecken MD, and Theis FJ (2019). Current best practices in single-cell RNAseq analysis: a tutorial. Molecular systems biology 15, e8746. 10.15252/msb.20188746. [PubMed: 31217225]

Highlights

- Tff2 marks transit-amplifying progenitors (TAP) that help sustain pancreatic homeostasis
- Tff2+ TAPs are susceptible to injury and resistant to PDAC initiation
- Pancreatitis converts $Kras^{mutant}$ $Tff2^{+}$ TAPs into CSC-like cells, promoting tumorigenesis
- Tff2+ TAP are protective against Kras-driven tumorigenesis through TFF2 secretion

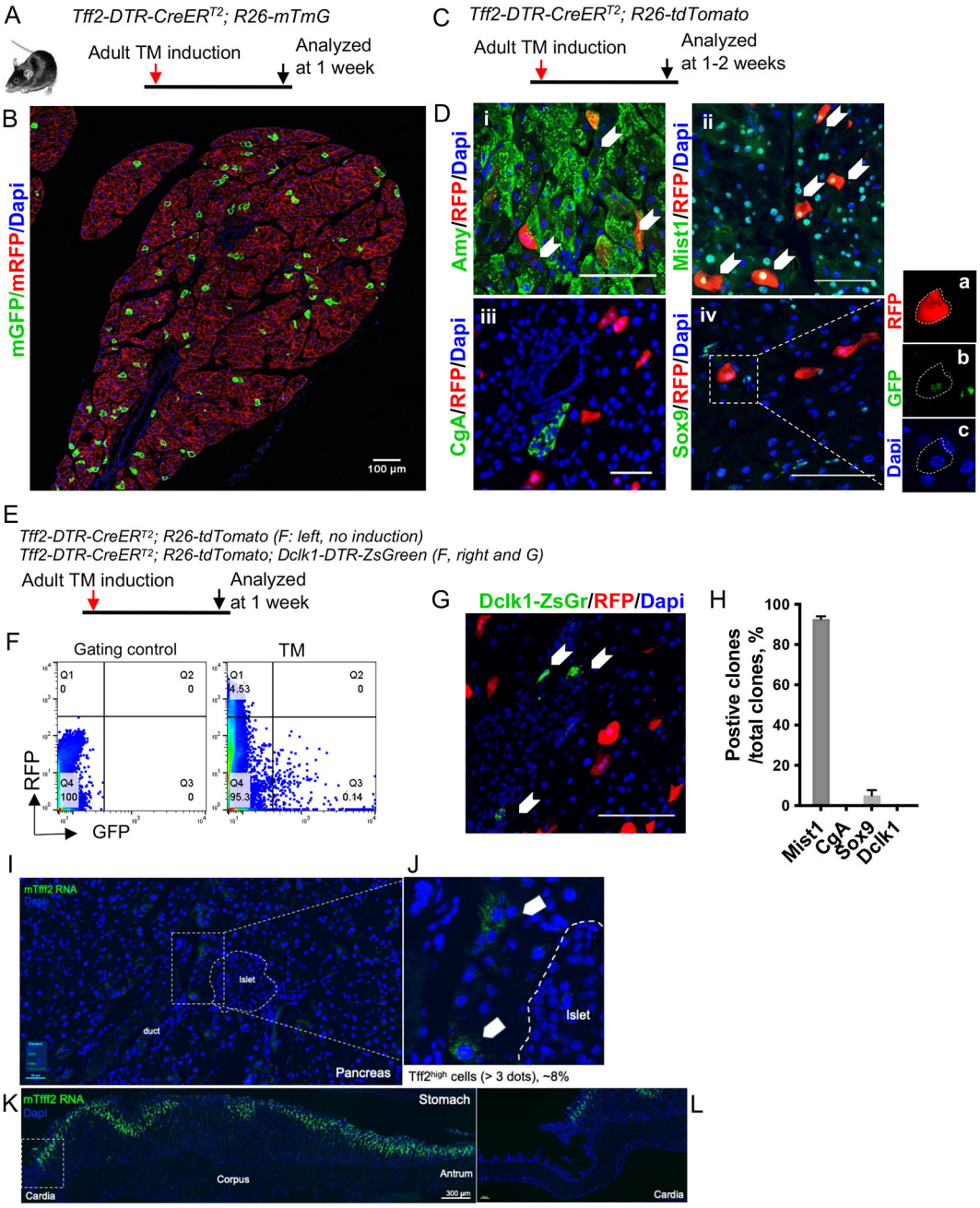

Figure 1. Tff2 labels a subset of pancreatic acinar population that is distinct from Dclk1 FPs

(A) Scheme of the protocol and animals. TM: 6 mg for each mouse.

(B) A representative fluorescent image of a small pancreatic lobe in *Tff2-DTR-CreER^{T2}; R26-mTmG mice*.

(C) Scheme of the protocol and animals. TM: 6 mg for each mouse.

(D) Representative immunofluorescent staining images of the pancreas in *Tff2-DTR-CreER^{T2}; R26-tdTomato* mice by amylase (i), Mist1(ii), chromogranin A (CgA, iii), and Sox9 (iv); n≥3. Arrows indicate double-positive cells. Insets from (iv−a, −b, and −c) show low expression of Sox9 in some of the Tff2 labeled cells.

(E) Scheme of the protocol and animals. TM: 6 mg for each mouse.
(F) FACS analysis of the pancreas in *Tff2-DTR-CreER^{T2}; R26-tdTomato; Dclk1-DTR-ZsGreen* mice (n>3, right) displaying no overlapping between these two populations. Left: gating control, *Tff2-DTR-CreERT2*; *R26-tdTomato* with no TM induction.
(G) A representative fluorescent image of the pancreas in *Tff2-DTR-CreER^{T2}; R26-tdTomato; Dclk1-DTR-ZsGreen* mice showing no co-labeling of Tff2^{+} cells with Dclk1^{+} cells (Arrows, n≥3).
(H) Quantification of double-positive cells (n≥3) from D-ii, D-iii, D-iv, and G.
(I-L) Representative images of ISH (RNAscope®) analysis on pancreas and stomach in WT mice (n=2–3), showing expression of Tff2 mRNA in acinar cells but absent in islets of the pancreas (I: zoom out Tff2^{+} acinar cells), and strong expression in the stomach (positive control, K: cardia region showing negative signals).
Scale bar in (B), (D), (G): 100 μm; (I) (K): 300 μm.
Data in (H) are represented as mean ± SEM.
See also Figure S1.

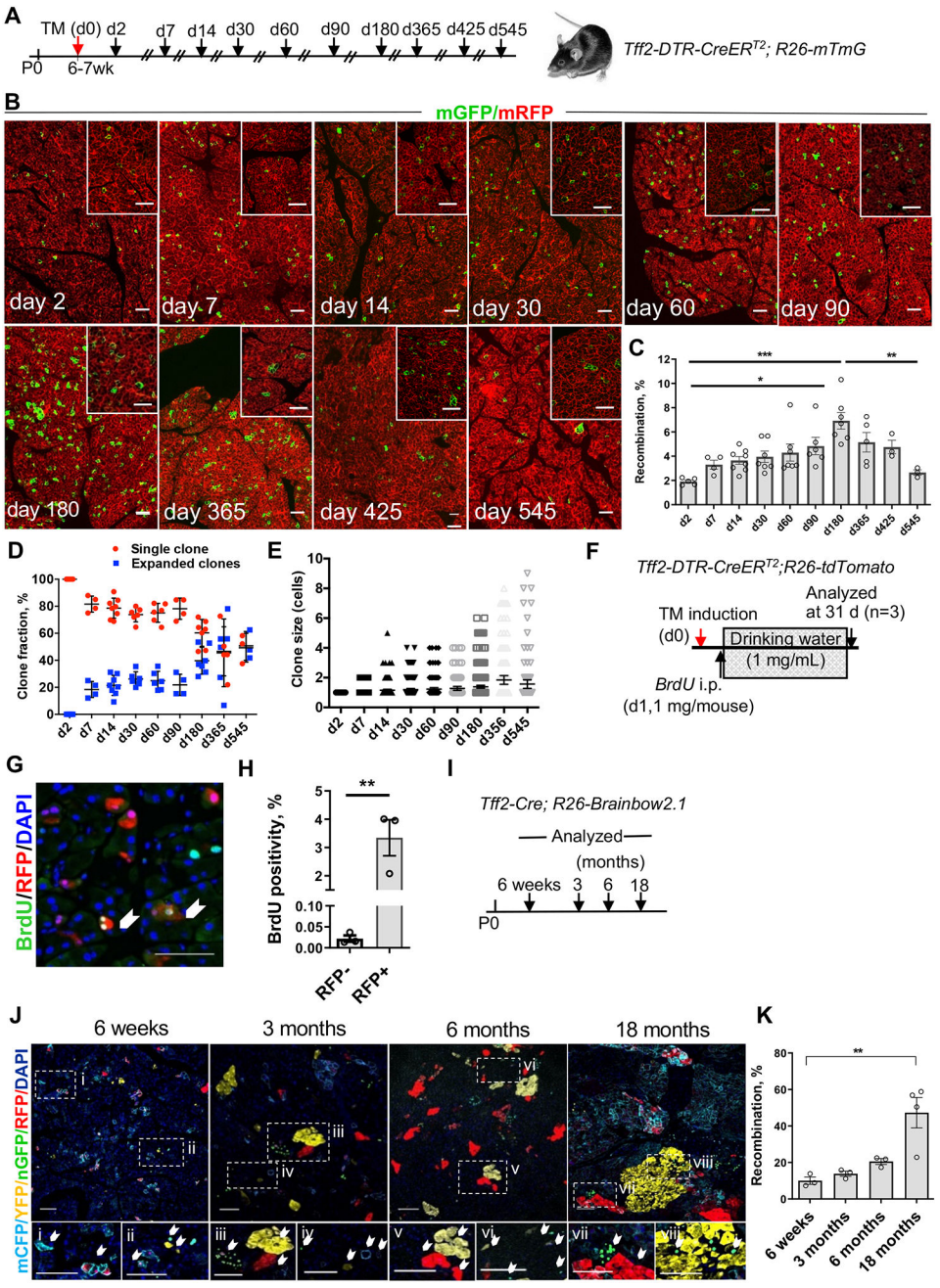

Figure 2. ***Tff2-DTR-CreER^{T2}*** **targets transit-amplifying progenitors (TAPs)**

(A) Scheme of the protocols and animals. TM: 6 mg for each mouse.

(B) Representative fluorescent images of time-course lineage-tracing experiments in the pancreas of *Tff2-DTR-CreER^{T2}; R26-mTmG* mice (n=3–8). Insert images are from different mice at the same time point.

(C) Quantification of recombined cells in (B) (n=3–8).

(D) Quantification of single and expanded clones in (B) (n=3–8).

(E) Quantification of clone size in (B) (n=3–8).

(F) Scheme of the protocol and animals. TM: 6 mg for each mouse.

(G) A representative immunofluorescent co-staining image of *BrdU* and RFP (arrows: double-positive cells).
(H) Quantification of *BrdU* positivity (n=3).
(I) Scheme of the protocol and animals.
(I) Representative fluorescent images from *Tff2-Cre; R26-Brainbow2.1* mice showing increased recombined cells from 6 weeks to 18 months (n=3–4).
(J) Quantification of the clusters and single clones from the mice in (H) (n=3–4).
Scale bar in (B), (G), (J): 100 μm
Data in (C), (D), (E), (H), (K) are represented as mean ± SEM.
Statistics: (C), (K): One-way ANOVA with post hoc Tukey's multiple comparisons. (H): Student's *t*-test (two-tailed).
See also Figure S2.

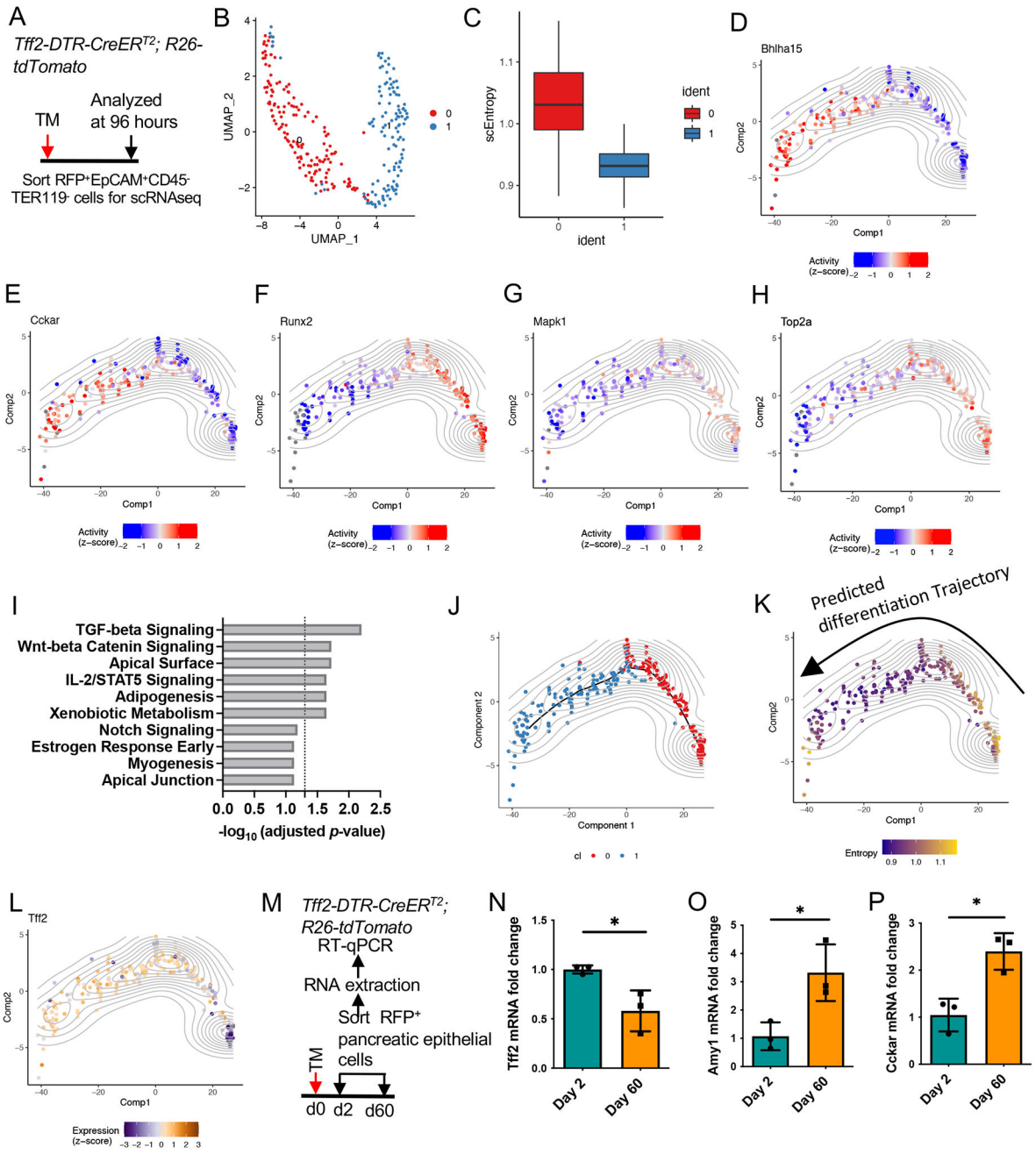

Figure 3. Molecular characterization of the Tff2$^+$ population by sing-cell RNA sequencing

(A) Scheme of the protocol and animals. TM: 6 mg for each mouse.

(B) A UMAP plot of unsupervised cluster analysis based on VIPER-inferred protein activity showing Tff2-expressing cells.

(C) A boxplot of the distribution of ScEntropy scores of Tff2-expressing cells in (B).

((D-H) Monocle-plots of VIPER-inferred protein activity of Bhlh15, Cckar, Runx2, Mapk1 and Top2A in the pseudotrajectory space.

(I) GO enrichment analysis of top differential VIPER-inferred protein activity in cluster 0. *P*-values were adjusted for multiple tests using the Benjamini-Hochberg procedure. The red dashed line indicates the *p*-value threshold of 0.05.
(J) A monocle-plot of pseudotrajectory distribution of cells in clusters 0 and 1 computated based on VIPER-inferred protein activity.
(K) A monocle-plot of scEntropy scores in the pseudotrajectory space.
(L) A monocle-plot showing the gene expression levels (z-scores) of Tff2-expressing cells in the pseudotrajectory space.
(M) Scheme of the protocol with animals. TM: 6 mg for each mouse.
(N-P) RT-qPCR analysis of sorted cells from (M), Student's *t*-test (two-tailed).
See also Figure S3.

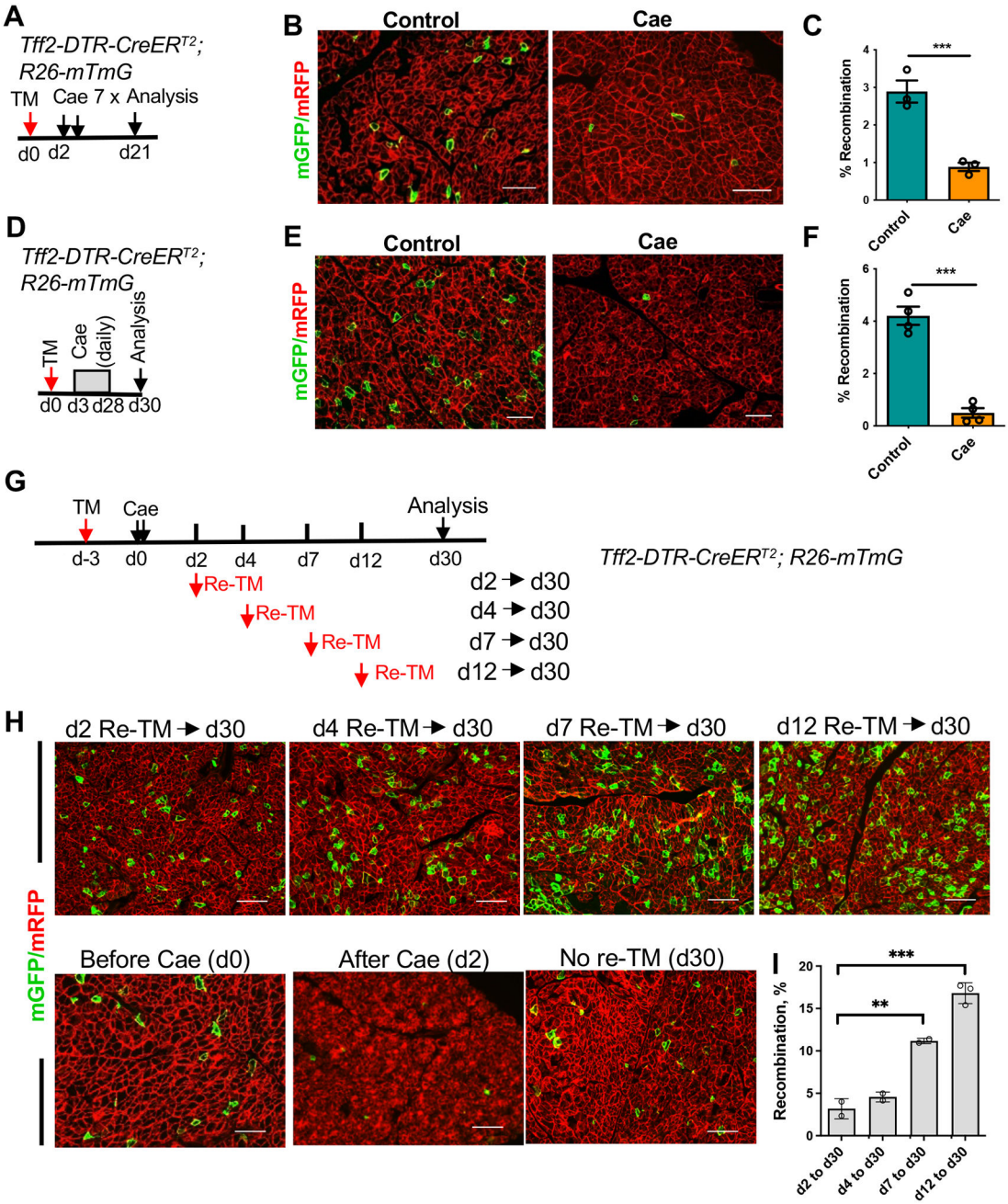

Figure 4. Pre-existing Tff2^{+} cells are susceptible to injury but are eventually replenished

(A) Scheme of the protocol and animals. TM: 6 mg for each mouse.

(B) Representative fluorescent images of *Tff2-DTR-CreER^{T2}; R26-mTmG* mice subjected to PBS (Control) or caerulein treatment as illustrated in (A) (n=3, male).

(C) Quantification of the recombination in (B) (n=3, male).

(D) Scheme of the protocol and animals. TM: 6 mg for each mouse.

(E) Representative fluorescent images of *Tff2-DTR-CreER^{T2}; R26-mTmG* mice subjected to PBS (Control) or caerulein treatment as illustrated in (D) (n=4, male).

(F) Quantification of the recombination in (E) (n=4, male).

(G) Scheme of TM + Caerulein + re-TM protocol. TM: 6 mg for each mouse.
(H) Representative images of *Tff2-DTR-CreER^{T2}; R26-mTmG* mice subjected to TM + caerulein + Re-TM protocol as illustrated in (G) (n=2–3, female). Additional images of pancreas in mice subjected to before, after, or no re-TM treatment were used as controls.
(I) Quantification of the recombination from the experiment in (H) (n=2–3, female).
Scale bar in (B), (E), (H): 100 μm.
Data in (C), (F), (I) are represented as mean ± SEM.
Statistics: (C), (F): Student's *t*-test (two-tailed). (I): One-Way ANOVA with post hoc Dunnett's multiple comparisons.
See also Figure S4.

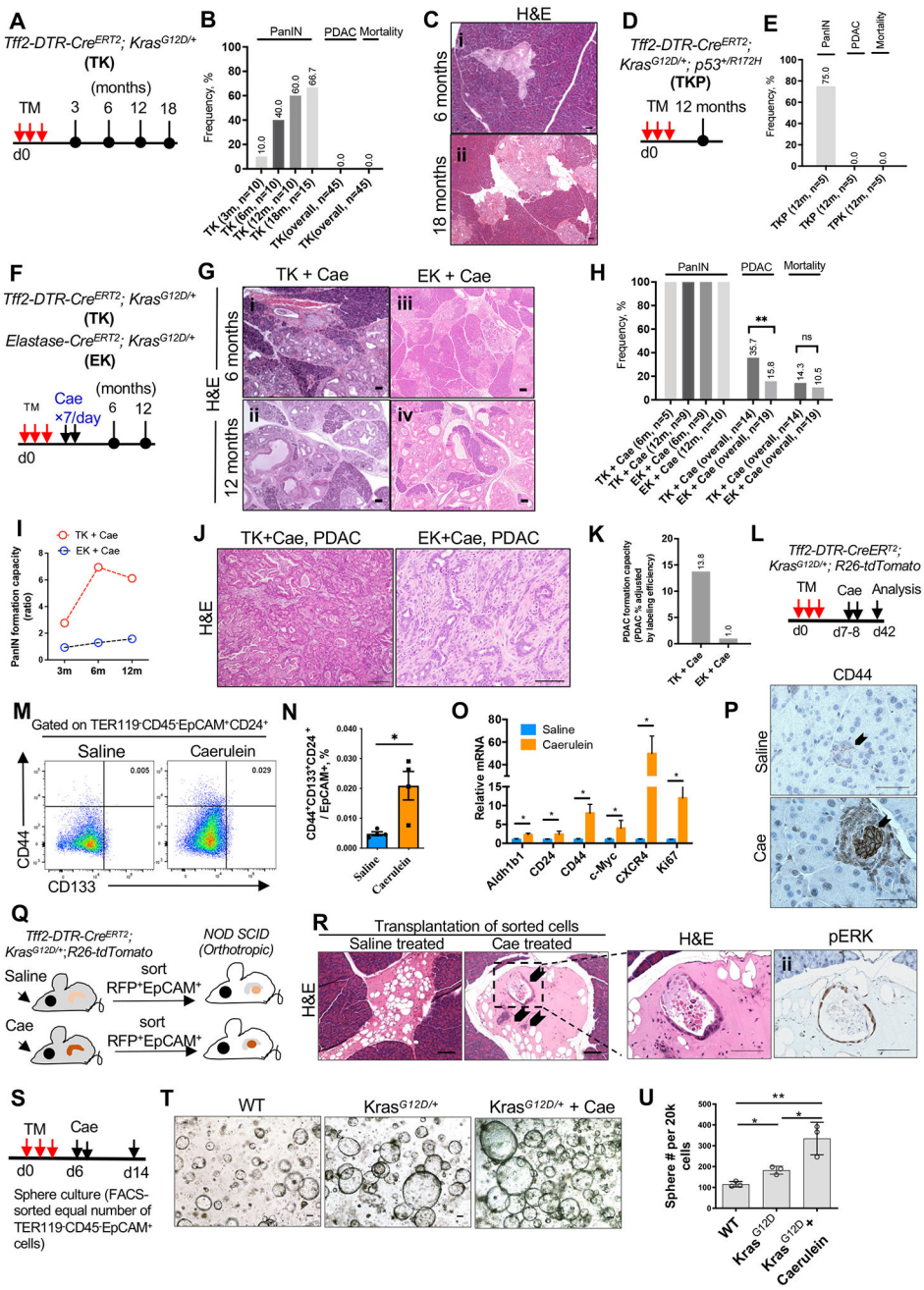

Figure 5. Tff2^{+} TAPs are resistant to oncogenic Kras^{G12D}-induced PDAC formation but acquire the oncogenic potential following pancreatitis

(A) Scheme of the protocols and animals. TM: 6 mg x3 for each mouse.

(B) Quantification of frequency of PanINs, PDAC and mortality in (A).

(C) Representative HE images of PanINs at 6 and 18 months after TM induction.

(D) Scheme of the protocols and animals. TM: 6 mg x3 for each mouse.

(E) Quantification of frequency of PanINs, PDAC and mortality in (D).

(F) Scheme of the protocols and animals. TM: 6 mg x3 for each mouse.

(G) Representative HE images of PanINs at 6 and 12 months after TM induction in TK + Cae and EK + Cae mice.

(H) Quantification of frequency of PanINs, PDAC and mortality in (F).
(I) Quantification of PanIN formation capacity.
(J) Representative HE images of PADC in TK + Cae and EK + Cae mice.
(K) Quantification of the ratio of PADC frequency adjusted by lineage tracing efficiency (PDAC formation capacity, also see supplementary Table 1).
(L) Scheme of the protocol and animals. TM: 6 mg x3 for each mouse.
(M) Representative FACS plots of CSC population in animals in (L).
(N) Quantification of data in (B) (n=4).
(O) RT-qPCR analysis of genes related to CSC and proliferation in pancreas in mice subjected to (A) (n=4).
(P) Representative IHC images of CD44 in the pancreas in mice in (L). Arrows indicate CD44 positive cells (n=4).
(Q) Scheme of the protocol and animals.
(R) Representative HE images of the pancreas of the NOD SCID mice transplanted with cells in (Q) (n=3–4). The insets show HE and IHC images of pERK. See method for details.
(S) Scheme of the protocol. TM: 6 mg x3 for each mouse.
(T) Sphere culture experiments of FACS-sorted equal number of $TER119^{-}CD45^{-}EpCAM^{+}$ cells from WT, or *Tff2-DTR-CreER*^{T2}*; Kras*$^{G12D/+}$ mice with or without caerulein in (S).
(U) Quantification of data in (T) (n=3).
Scale bar in (E), (G), (I), (P), (R), (T): 100 μm
Data in (N), (O), and (U) are represented as mean ± SEM.
Statistics: (H): Differences between groups Tff2 + Cae and Ela + Cae were analyzed using two-sided *Chi*-square test. (N), (O): Student's *t*-test (two-tailed). (U): One-Way ANOVA with post hoc Tukey's multiple comparisons
See also Figure S5 and S6.

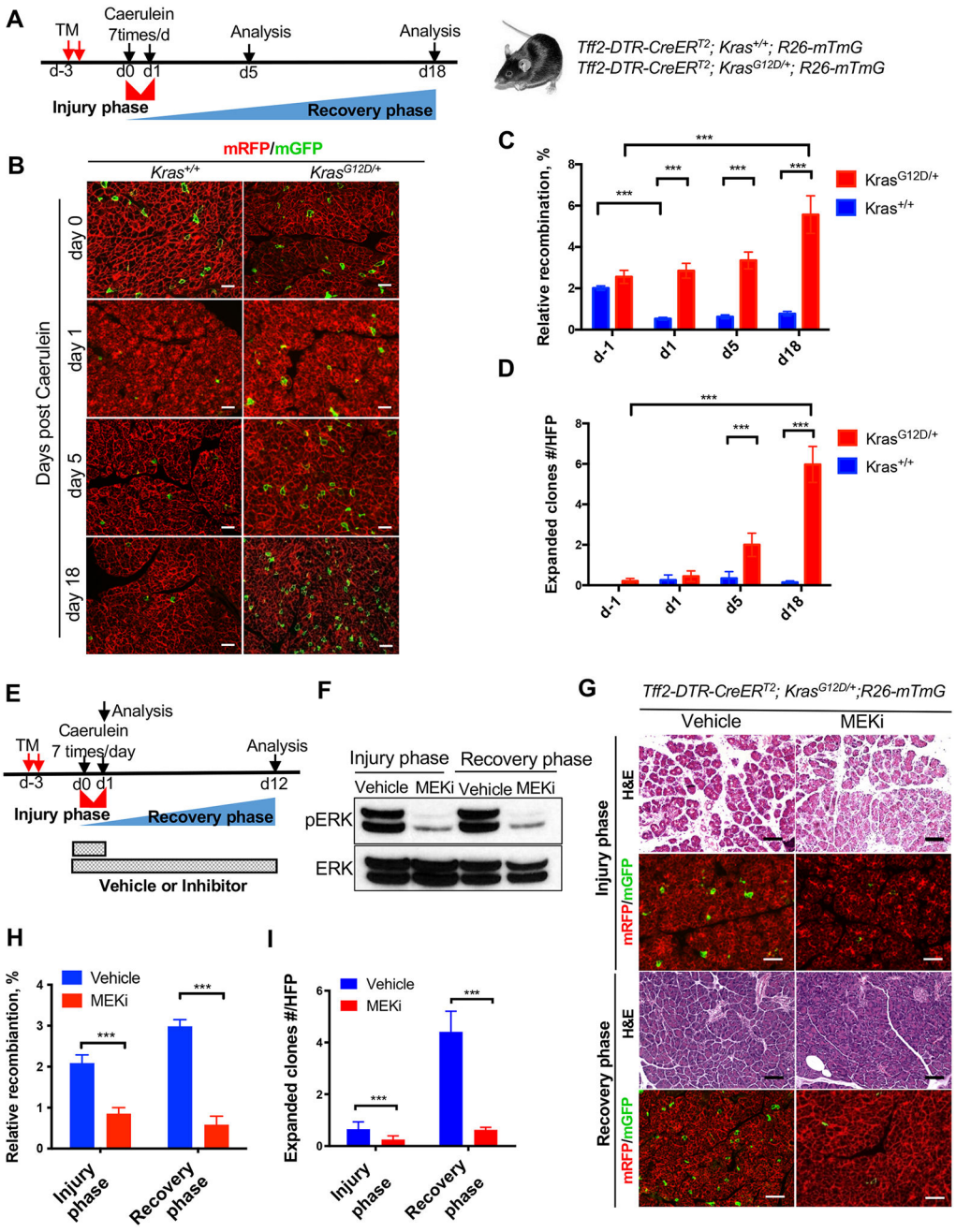

Figure 6. Oncogenic Kras prevents Tff2$^+$ TAPs from caerulein-induced depopulation

(A) Scheme of the protocol. TM: 6 mg x2 for each mouse.

(B) Representative fluorescent images of *Tff2-DTR-CreER^{T2}; Kras$^{+/+}$; R26-mTmG* or *Tff2-DTR-CreER^{T2}; Kras$^{G12D/+}$; R26-mTmG* mice subjected to the protocol in (A) (n=3–4, male).

(C) Quantification of the mGFP recombination in (B) (n=3–4, male).

(D) Quantification of the expanded clones in (B) (n=3–4, male).

(E) Scheme of the protocol. TM: 6 mg x2 for each mouse.

(F) Representative Western blotting images of the pancreas in mice subjected to the protocol in (E) (n=3–4, male). MEKi: MEK inhibitor.
(G) Representative HE and fluorescent images of *Tff2-DTR-CreER^{T2}; Kras$^{G12D/+;}$ R26-mTmG* mice subjected to the protocol in (E) (n=3–4, male).
(H) Quantification of the mGFP recombination in (G) (n=3–4, male).
(I) Quantification of the expanded clones in (G) (n=3–4, male).
Scale bar in (B), (G): 100 μm
Data in (C), (D), (H), and (I) are represented as mean ± SEM.
Statistics: (C), (D): Two-Way ANOVA with post hoc Tukey's multiple comparisons. (H), (I): Student's *t*-test (two-tailed).

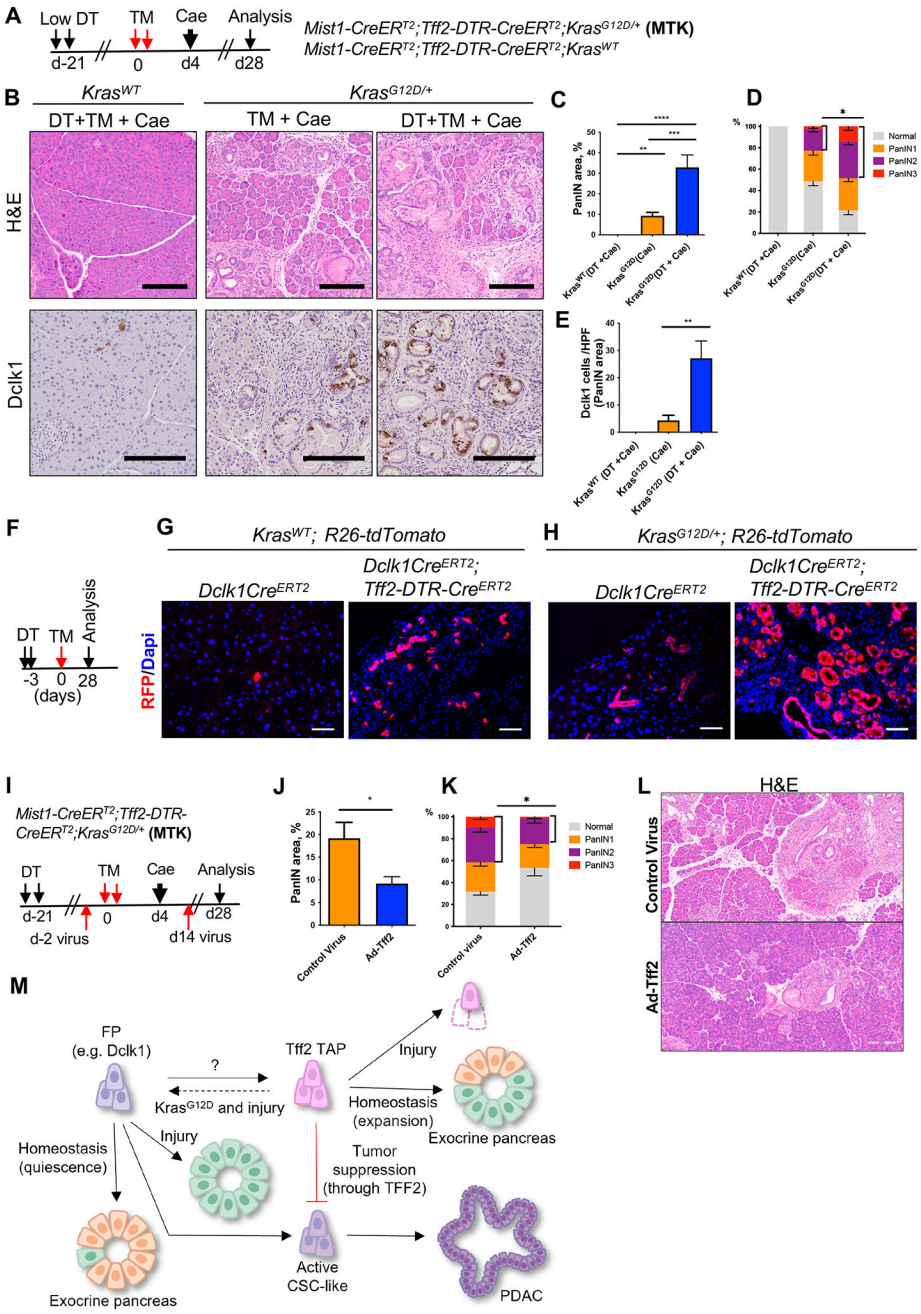

Figure 7. Tff2^{+} TAPs are protective against Kras-driven tumorigenesis

(A) Scheme of the protocol and animals. TM: 6 mg x2 for each mouse.

(B) Representative HE and IHC images (Dclk1) of the pancreas in mice subjected to the protocol (A). *Tff2-DTR-CreER^{T2}; Kras$^{+/+}$* mice were subjected to DT + TM + Cae. *Tff2-DTR-CreER^{T2}; Kras$^{G12D/+}$* mice were subjected to TM + Cae or DT + TM + Cae (n=6–7).

(C and D) Quantification of PanIN area and scores in (A) and (B) (n=6–7).

(E) Quantification of Dclk1 IHC staining in (A) and (B) (n=6–7).

(F) Scheme of the protocol. TM: 6 mg x2 for each mouse.

(G) Representative fluorescent images of *Dclk1-CreER^{T2}; R26-tdTomato* or *Tff2-DTR-CreER^{T2}; Dclk1-CreER^{T2}; R26-tdTomato* mice subjected to the protocol in (F) (n≥3).
(H) Representative fluorescent images of *Dclk1-CreER^{T2}; Kras$^{G12D/+}$; R26-tdTomato* or *Tff2-DTR-CreER^{T2}*; *Dclk1-CreER^{T2}; Kras$^{G12D/+}$; R26-tdTomato* mice subjected to the protocol in (F) (n≥3).
(I) Scheme of the protocol and animals. TM: 6 mg x2 for each mouse.
(J-K) Quantification of PanIN area and scores (n=7).
(L) Representative HE images of the pancreas in mice subjected to protocol in (I).
(M) Illustration of 2-progenitor hypothesis.
Scale bar in (B), (L): 200 μm; (G), (H): 100 μm
Data in (C), (D), (E), (J), (K) are represented as mean ± SEM.
Statistics: (C), (E): One-Way ANOVA with post hoc Tukey's multiple comparisons. (D), (J), (K): Student's *t*-test (two-tailed).
See also Figure S7.

Key resources table

REAGENT or RESOURCE	SOURCE	IDENTIFIER
Antibodies		
Rabbit monoclonal anti-phosphorylated ERK	Cell Signaling Technology	Cat# 9101S; RRID: AB_331646
Rabbit polyclonal anti-ERK	Cell Signaling Technology	Cat# 4695S; RRID: AB_390779
Biotinylated goat anti-rabbit IgG	Vector Laboratories	Cat# BA-1000; RRID: AB_2313606
Donkey Anti-Rabbit IgG, HRP-Linked Whole Ab	GE Healthcare Life Sciences	Cat# NA-934; RRID: AB_772206
Rabbit monoclonal anti-Mist1	Gifted by Dr. Stephen Konieczny[66]	N/A
Rat APC anti-mouse CD326 (Ep-CAM)	BioLegend	Cat# 118214; RRID: AB_1134102
Rabbit Anti-Amylase, alpha Antibody	Sigma-Aldrich	Cat# A8273, RRID: AB_258380
Anti-SOX9 antibody	Abcam	Cat# ab185966; RRID: AB_2728660
Rabbit Anti-Chromogranin A Polyclonal Antibody	Abcam	Cat# AB15160, RRID: AB_992780
Rabbit Anti-DCAMLK1 Polyclonal Antibody	Abcam	Cat# ab31704, RRID: AB_873537
Rat Anti-BrdU Monoclonal Antibody	Abcam	Cat# ab6326, RRID: AB_305426
Rabbit polyclonal anti-Ki67	Abcam	Cat# ab15580; RRID: AB_443209
Rabbit polyclonal Cytokeratin 19 antibody	Abcam	Cat# ab15463, RRID: AB_2281021
Rabbit Anti-RFP Antibody	Rockland	Cat# 600-401-379, RID: AB_2209751
Rabbit Anti-Claudin 18 Polyclonal Antibody	Thermo Fisher Scientific	Cat# 38-8100, RRID: AB_2533383
Pacific Blue™ anti-mouse TER-119/Erythroid Cells antibody	BioLegend	Cat# 116232, RRID: AB_2251160
Polyclonal anti-p53 antibody	Leica (gifted by Dr. Wu Gu)	Cat# p53-CM5p, RID: AB_2744683
Pacific Blue™ anti-mouse CD45 antibody	BioLegend	Cat# 103126, RRID: AB_493535
APC anti-mouse CD133 antibody	BioLegend	Cat# 141207, RRID: AB_10898121
PE/Cy7 anti-mouse/human CD44 antibody	BioLegend	Cat# 103030, RRID: AB_830787
APC/Cyanine7 anti-mouse CD326 (Ep-CAM) antibody	BioLegend	Cat# 118217, RRID: AB_1501158
FITC anti-mouse CD24 Antibody	BD Biosciences	Cat# 561777, RRID: AB_10896486
APC Anti-mouse CD133	Thermo Fisher Scientific	Cat# 17-1331-81, RRID: AB_823120
PE-Cy5 Anti-mouse CD45	Thermo Fisher Scientific	Cat# 15-0451-81, RID: AB_468751
PE-Cy5 anti-mouse TER-119/Erythroid Cells antibody	Thermo Fisher Scientific	Cat# 15-5921-81, RID: AB_468809
FITC Anti-human CD49f	BD Biosciences	Cat# 561893, RRID: AB_10894397
Anti-CD45 antibody	Abcam	Cat#: ab10558, RRID: AB_442810
Anti-Cytokeratin 19 antibody	Abcam	Cat#: ab52625, RRID: AB_2281020
F4/80 (D2S9R) XP® Rabbit mAb	Cell Signaling Technology	Cat#: 70076S, RRID: AB_2799771
Anti-E Cadherin (DECEMA1)	Abcam	Cat#: ab15112, RRID: AB_2070016
Anti-PDX1 antibody	Abcam	Cat#: ab47267, RRID: AB_777179
Bacterial and virus strains		
Biological samples		

REAGENT or RESOURCE	SOURCE	IDENTIFIER
Chemicals, peptides, and recombinant proteins		
Fetal Bovine Serum	Gibco	Cat# 16140071
RBC Lysis Buffer (10X)	BioLegend	Cat# 420301
Collagenase, Type V	MilliporeSigma	Cat# C9263
DNase I	Roche Diagnostics	Cat# 3724778103
N-2 Supplement	Gibco	Cat# 17502048
B-27 Supplement	Gibco	Cat# 17504044
Nu-serum IV	Corning	Cat# 355104
Cholera Toxin from Vibrio Cholerae	MilliporeSigma	Cat# C8052
Trypsin Inhibitor from Glycine Max	MilliporeSigma	Cat# T6522
DAPI Solution	BD Pharmingen	Cat# 564907
HBSS - Hank's Balanced Salt Solution	Gibco	Cat# 14175079
BD Horizon BrilliantTM Stain Buffer	BD Biosciences	Cat# 563794
Normal Goat Serum Blocking Solution	Vector Laboratories	Cat# S-1000
Bovine Serum Albumin	MilliporeSigma	Cat# A9418
TritonX-100	Fisher Scientific	Cat# BP151-500
TWEEN 20	Sigma-Aldrich	Cat# P1379
Dimethyl Sulfoxide	Sigma-Aldrich	Cat# D8418
Penicillin Streptomycin	Gibco	Cat# 15140122
ProLong® Gold Antifade Mountant	Thermo Fisher Scientific	Cat# P36934
VECTASHIELD Antifade Mounting Medium with DAPI	Vector Laboratories	Cat# H-1200
Y-27632	Selleck Chemicals	Cat# S1049
RNA*later* stabilization solution	Ambion	Cat# AM7020
5-Bromo-2′-deoxyuridine	MilliporeSigma	Cat# B5002-100MG
Tamoxifen	MilliporeSigma	Cat# T5648
Trametinib	Selleckchem	Cat# S2673
Caerulein ammonium salt	Bachem	Cat# 4030451.0005
Diphtheria Toxin	EMD Millipore	Cat# 322326-1MG
Diphtheria Toxin	Sigma-Aldrich	Cat# D0564-1MG
Dexamethasone	Sigma-Aldrich	Cat# D2915-100MG
Critical commercial assays		
Mouse Trefoil Factor 2 ELISA Kit, 96-Strip-Wells	MyBioSource	Cat# MBS763147
SuperScript III First-Strand Synthesis System	Thermo Fisher Scientific	Cat# 18080051
FastStart Universal SYBR Green Master (Rox)	Roche Molecular Systems	Cat# 4913850001
Liquid DAB+ Substrate Chromogen System	Dako	Cat# K3468
RNeasy Micro Kit	QIAGEN	Cat# 74004
ECL Western Blotting Detection Reagents	Amersham	Cat# RPN2209

REAGENT or RESOURCE	SOURCE	IDENTIFIER
Bicinchoninic acid (BCA) kit	Thermo Fisher Scientific	Cat# 15045
SignalStain® Boost IHC Detection Reagent	Cell Signaling Technology	Cat# 8114
Deposited data		
Singe-cell RNAseq data of Tff2+ cells from mouse pancreas		GEO: GSE236377
Experimental models: Cell lines		
Experimental models: Organisms/strains		
Mouse: C57BL/6J	The Jackson Laboratory	Stock No: 000664
Mouse: NOD.CB17-Prkdcscid/J	The Jackson Laboratory	Stock No: 001303
Mouse: Rosa26-tdTomato: Gt(ROSA)26Sortm9(CAG-tdTomato)Hze/J	The Jackson Laboratory	Stock No: 007909
Mouse: Rosa26-mT/mG: Rosa26-B6.129(Cg)-Gt(ROSA)26Sortm4(ACTB-tdTomato,-EGFP)Luo/J	The Jackson Laboratory	Stock No:007676
Mouse: Rosa26-Brainbow2.1: B6.129P2-Gt(ROSA)26Sortm1(CAG-Brainbow2.1)Cle/J	The Jackson Laboratory	Stock No: 017492
Mouse: LSL-Trp53$^{+/R172H}$: B6.129S4(Cg)-Trp53$^{tm2.1Tyj}$/J	The Jackson Laboratory	Stock No: 008183
Mouse: LSL-Kras$^{+/LSL-G12D}$: B6.129S4-Kras^{tm4Tyj}/J	The Jackson Laboratory	Stock No: 008179
Mouse: Pdx-Cre: B6.FVB-Tg(Pdx1-cre)6Tuv/J	The Jackson Laboratory	Stock No: 014647
Mouse: Mist1-CreERT2: B6.129-hlha15$^{tm3(cre/ERT2)Skz}$/J	The Jackson Laboratory	Stock No: 029228
Mouse: Dclk1-CreERT2 (Line 4)	This study, the same founder of Westphalen et al.[9]	Stock No. 911950
Mouse: Tff2-Cre	Hayakawa et al.[67]	Stock No. 913314
Mouse: Dclk1-DTR-ZsGreen	This study	Stock No. 403549
Mouse: Elastase-CreERT2	Steven Konieczny (Purdue)	N/A
Mouse: Tff2-DTR-CreERT2	This study	Stock No. 400325
Oligonucleotides		
Recombinant DNA		
Software and algorithms		
ImageJ version1.6/Fiji	NIH	http://imagej.net
FlowJo V10	FlowJo	https://www.flowjo.com
R-3.6.1	Bell Laboratories	https://www.r-project.org/about.html
10X CellRanger software: version 1.3.0	10X Genomics	https://support.10xgenomics.com/singlecell-gene-expression
GraphPad Software	GraphPad Software	http://graphpad.com
R for Statistical Programming	R-Core-Team (2022)[68]	https://www.R-project.org

REAGENT or RESOURCE	SOURCE	IDENTIFIER
ARACNe	Lachmann et al.[69]	https://github.com/califano-lab/ARACNe-AP
VIPER	Alvarez et al.[39]	https://bioconductor.org/packages/release/bioc/html/viper.html
Seurat	Hao et al.[70]	https://satijalab.org/seurat/
Cluster	Martin Maechler et al.[71]	https://cran.r-project.org/web/packages/cluster/index.html
ComplexHeatmap	Gu et al.[72]	https://bioconductor.org/packages/release/bioc/html/ComplexHeatmap.html
EnrichR	Zhuorui Xie et al.[73]	https://maayanlab.cloud/Enrichr/
Monocle	Trapnell et al. [74]	http://cole-trapnell-lab.github.io/monocle-release/
ggplot2	Wickham et al.[75]	https://ggplot2.tidyverse.org
SLICE	Guo et al.[76]	https://github.com/xu-lab/SLICE
Other		